A polyconvex transversely-isotropic invariant-based formulation for electro-mechanics: Stability, minimisers and computational implementation

Martin Horák[a],[*], Antonio J. Gil[b], Rogelio Ortigosa[c], Martin Kružík[d]

[a] *Faculty of Civil Engineering, Czech Technical University, Thákurova 7, CZ-166 29 Praha 6, Czech Republic*
[b] *Zienkiewicz Centre for Computational Engineering, Faculty of Science and Engineering, Swansea University, Bay Campus, SA1 8EN, United Kingdom*
[c] *Computational Mechanics and Scientific Computing Group, Technical University of Cartagena, Campus Muralla del Mar, 30202, Cartagena (Murcia), Spain*
[d] *Czech Academy of Sciences, Institute of Information Theory and Automation, Pod vodárenskou věží 4, CZ-182 00 Praha 8, Czech Republic*

Abstract

The use of Electro-Active Polymers (EAPs) for the fabrication of evermore sophisticated miniaturised soft robotic actuators has seen an impressive development in recent years. The incorporation of crystallographic anisotropic micro-architectures, within an otherwise nearly uniform isotropic soft polymer matrix, has shown great potential in terms of advanced three-dimensional actuation (i.e. stretching, bending, twisting), especially at large strains, that is, beyond the onset of geometrical pull-in instabilities. From the computational point of view, the design of accurate and robust albeit efficient constitutive models is a very active area of research. This paper introduces a novel polyconvex phenomenological invariant-based transversely isotropic formulation (and relevant computational frameworks) for the simulation of transversely isotropic EAPs at large strains, where the *ab initio* satisfaction of polyconvexity is exploited to ensure the robustness of numerical results for any range of deformations and applied electric fields. The paper also presents key important results both in terms of the existence of minimisers and material stability of coupled electro-mechanics, enhancing previous works in the area of large strain elasticity. In addition, a comprehensive series of selected numerical examples is included in order to demonstrate the effect that the anisotropic orientation and the contrast of material properties, as well as the level of deformation and electric field, have upon the response of the EAP when subjected to large three-dimensional stretching, bending and torsion, including the possible development of wrinkling and the potential loss of ellipticity in ill-posed constitutive models.
© 2022 Elsevier B.V. All rights reserved.

Keywords: Polyconvexity; Transversely isotropic; Dielectric elastomers; Electro-elasticity; Finite element method

1. Introduction

Electro-Active Polymers (EAPs) are a type of soft smart materials capable of displaying significant change in shape in response to electrical stimuli. EAPs have been thoroughly studied over the years [1–4] and dielectric

---

* Corresponding author.

E-mail addresses: martin.horak@cvut.cz (M. Horák), a.j.gil@swansea.ac.uk (A.J. Gil), rogelio.ortigosa@upct.es (R. Ortigosa), kruzik@utia.cas.cz (M. Kružík).

elastomers are recognised as one of the most popular EAPs [5–7] due to their outstanding actuation capabilities[1] (i.e., lightweight, fast response time, flexibility, low stiffness properties), which makes them ideal for their use as soft robots [1,2,9–15], flexible energy generators [16,17] or tunable optics [18,19]. However, a large electric field is still generally required in order to access the large actuation regime in EAPs, an aspect that very often places them at risk of electromechanical pull-in instabilities or even electrical breakdown [20].

It was shown in [21] that fibre reinforcement can suppress the electro-mechanical pull-in instability and improve EAPs' applicability. A dielectric elastomer stiffened with fibres in the hoop direction leading to large, voltage-induced deformations was proposed in [22]. In [23], a voltage-driven deformation of dielectric elastomer reinforced with a family of helical fibres leading to torsional behaviour is studied and the effect of fibre orientation on the actuation of a fibre-reinforced bending actuator is analysed in [24].

In order to reduce the operational voltage required for actuation in EAPs, some authors have advocated for the design of composite-based EAPs [25–27], typically combining an ultra-soft and low-permittivity elastomer matrix with a stiffer and high-permittivity inclusion [27–30]. Due to the continuous improvement in layer-by-layer fabrication techniques [31], multi-layered laminated EAP composites have gained popularity. From the modelling point of view, Refs. [4,20,32–38] have demonstrated that the contrast between the properties of the composite constituents is one of their critical design factors, where the actuation performance of an EAP composite subjected to simple in-plane stretching can be amplified by several orders of magnitude with respect to that of a single-phase EAP, even in the linearised regime.

The use of computational methods constructed on the basis of variational principles is nowadays acknowledged as the preferred method for the in-silico simulation of complex actuation. Building upon the works of Toupin [39,40] and Dorfmann, Ogden, MacMeeking, Suo, and co-workers in [41–48], recent contributions in the field of computational electro-mechanics can be found in [49–52]. In these works, the constitutive behaviour of a single-phase electro-mechanical material is encoded within a carefully (phenomenologically) defined energy functional which depends upon appropriate strain measures, a Lagrangian electric variable and, if dissipative effects are considered, an electromechanical internal variable [53]. Bustamante et al. in [54,55] present an irreducible invariant basis for transversely isotropic EAPs (without piezoelectric effects) as well as several constitutive restrictions that the final energy density must be fulfilled, such as the Baker–Ericksen inequality [55].

However, in order to design and optimise EAPs for a specific application, a robust and reliable physics-based mathematical theory is needed. Despite great recent progress in the field of constitutive modelling of electro-active materials (see above), the polyconvexity condition [56], which represents a sufficient condition for a mathematically well-posed formulation, has been introduced only recently,[2] see [57–59]. In previous publications [57,58,60,61], the authors put forward a new computational framework for single-phase reversible electro-mechanics, where material stability is always ensured via the selection Convex Multi-Variable (CMV) energy densities, that is, convex with respect to the minors of the deformation gradient tensor ($\boldsymbol{F}$, $\boldsymbol{H}$, J), the Lagrangian electric displacement $\boldsymbol{D}_0$, and the spatial electric displacement $\boldsymbol{d} = \boldsymbol{F}\boldsymbol{D}_0$. CMV energy densities (generally referred to as *polyconvex* or $\mathcal{A}$-*polyconvex* [62]) guarantee existence of minimisers [62], ellipticity [57] in the quasi-static case and hyperbolicity in the dynamic case [58], thus precluding anomalous mesh dependency effects. The theory of polyconvexity for mechanical anisotropic energy densities was magnificently explored by Schröder and Neff [63] and it was also initially studied for electro-mechanics anisotropic energies in [64].[3]

As a result, the aim of this paper is three-fold. ***First***, the in-silico modelling of realistic three-dimensional deformation scenarios (namely, combined bending/torsion/stretching), way beyond the onset of geometrical instabilities and without the need to resort to any simplifications in the kinematics of the EAP (e.g., plane strain, exact incompressibility). ***Second***, the consideration of internal micro-architectures beyond the simpler single-phase isotropy, with focus on the very relevant transverse isotropy groups, with the idea of developing computationally efficient (phenomenological, invariant-based) constitutive models for EAPs, which could be in the future enriched by state-of-the-art data assimilation techniques [65]. ***Third***, to ensure the existence and material stability (ellipticity) of computer simulations by unifying and enhancing key results scattered in the literature. From the macroscopic

---

[1] It is worth noting that the maximum achieved voltage-induced area deformation of a dielectric elastomer has been 2200% [8].

[2] Note that, in the context of a boundary value problem, polyconvexity together with coercivity guarantees the existence of global minimisers.

[3] However, the differential constraint imposed by the Gauss's law was not accounted for, leading to an incomplete polyconvexity condition, omitting the coupled electro-mechanical contributions.

point of view, the loss of ellipticity leads to a mathematically and numerically ill-posed problem that needs to be regularised, e.g., by introducing higher-order derivatives into the constitutive law resulting in the so-called higher-order continua, see [66,67] for a recently proposed theory of gradient-polyconvexity. Such regularisation is out of the present article's scope and will be studied in a forthcoming publication.

From the **constitutive modelling standpoint**, this paper will apply polyconvexity, objectivity, and *isotropicisation*, in order to develop energy densities constructed on the basis of polyconvex invariants forming an irreducible basis for the characterisation of transversely isotropic EAPs. From the **numerical implementation standpoint**, Finite Element analysis of transversely isotropic EAPs will be presented using both the standard displacement-potential ($\boldsymbol{\phi}$, φ) variational principle and an enhanced mixed Hu–Washizu three-field type of formulation ($\boldsymbol{\phi}$, $\boldsymbol{D}_0$, φ). The high nonlinearity of the quasi-static electro-mechanical problem will be addressed via a monolithic Newton–Raphson scheme, with an arc length technique used to bypass geometrical instabilities. A tensor cross product operation between vectors and tensors [68,69] will be used to reduce the complexity of the algebra.

The outline of this paper is as follows. Section 2 describes the necessary elements of nonlinear continuum reversible electro-mechanics and some key variational principles. Section 3 focusses on the concept of polyconvexity as a basis for the description of phenomenological constitutive models for EAPs. The section starts with some generalised convexity conditions, before introducing the actual definition of polyconvexity or $\mathcal{A}$-polyconvexity (as referred to by Šilhavý [62], also referred as Multi-Variable Convexity by Gil and Ortigosa [57]). The section summarises and puts into context key results in terms of existence of minimisers [62] and material stability for coupled reversible electro-mechanics, beyond those of single mechanics [70]. Section 4 describes the basis for the anisotropic invariant-based constitutive models adopted in this work, where special attention is paid to the important crystallographic groups $\mathcal{D}_{\infty h}$ and $\mathcal{C}_{\infty}$ [71–73]. The section concludes by listing so-called polyconvex basis of invariants for the creation of polyconvex invariant-based constitutive models. Section 5 presents a series of numerical examples in order to assess the capabilities of the proposed model. Specifically, in a first example, a local analysis is conducted at a quadrature (Gauss point) level where the effect of orientation of anisotropy upon purely mechanical and electro-mechanical tests is presented. In the second example, complex three-dimensional bending/torsion/stretching combined modes of deformation are studied for a soft robot actuator, monitoring macroscopic stability, and observing the effect that anisotropy has in the predominance of a deformation mode against others. In the third example, the effect of anisotropy orientation on the development of wrinkling patterns in an EAP is studied. In the last example, complex three dimensional torsion is studied for a piezoelectric-type material along with the satisfaction of polyconvexity. Eventually, Section 6 provides some concluding remarks about the paper.

2. Nonlinear continuum electromechanics

This section briefly summarises the fundamental electro-mechanical equations governing the response of an Electro-Active Polymer (EAP) at large strains.

### 2.1. Kinematics: motion and deformation

Let us consider the deformation of an Electro-Active Polymer (EAP) (see Fig. 1) with reference configuration given by a bounded Lipschitz domain $\Omega_0 \subset \mathbb{R}^3$ with boundary $\partial \Omega_0$, and its unit outward normal $\boldsymbol{N}$. After the deformation, the EAP occupies an actual configuration given by a set $\Omega \subset \mathbb{R}^3$ with boundary $\partial \Omega$ and unit outward normal $\boldsymbol{n}$. If the deformation is continuous and bijective then Ω is also open. The deformation of the EAP is defined by a mapping $\boldsymbol{\phi} : \Omega_0 \to \mathbb{R}^3$ linking material particles $\boldsymbol{X} \in \Omega_0$ to $\boldsymbol{x} \in \Omega = \boldsymbol{\phi}(\Omega_0)$. Associated with $\boldsymbol{\phi}(\boldsymbol{X})$, the deformation gradient tensor $\boldsymbol{F}$ is defined as[4]

$$\boldsymbol{F} = \nabla_0 \boldsymbol{\phi}(\boldsymbol{X}) ; \qquad F_{iI} = \frac{\partial \phi_i}{\partial X_I}. \tag{2.1}$$

Related to $\boldsymbol{F}$, its co-factor $\boldsymbol{H}$ and its Jacobian J [69,74] are defined as

$$\boldsymbol{H} = \mathrm{Cof}\, \boldsymbol{F} = \frac{1}{2} \boldsymbol{F} \times \boldsymbol{F}; \qquad J = \det \boldsymbol{F} = \frac{1}{3} \boldsymbol{H} : \boldsymbol{F}, \tag{2.2}$$

---

[4] Lower case indices $\{i, j, k\}$ will be used to represent the spatial configuration, whereas capital case indices $\{I, J, K\}$ will be used to represent the material description. Zero as the lower index next to the nabla operator indicates that it is the referential gradient.
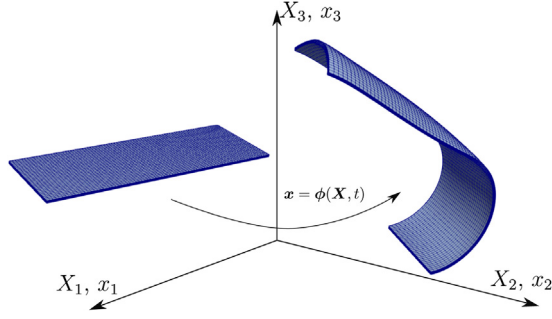
Fig. 1. Deformation mapping $\boldsymbol{\phi}(\boldsymbol{X})$.

with $(\boldsymbol{A} \times \boldsymbol{B})_{iI} = \mathcal{E}_{ijk}\mathcal{E}_{IJK}A_{jJ}B_{kK}$, $\forall \boldsymbol{A}, \boldsymbol{B} \in \mathbb{R}^{3 \times 3}$, where $\mathcal{E}_{ijk}$ (or $\mathcal{E}_{IJK}$) symbolises the third-order alternating tensor components and the use of repeated indices implies summation.[5] The deformation mapping is assumed to be sufficiently smooth, bijective and orientation preserving, so that $J > 0$ *a.e.* to avoid interpenetrability.

2.2. Governing equations in electro-mechanics

In the absence of inertial effects, the conservation of linear momentum (i.e. equilibrium) can be written in a Total Lagrangian fashion as

$$\text{DIV } \boldsymbol{P} + \boldsymbol{b}_0 = 0 \quad \text{in} \quad \Omega_0, \tag{2.3}$$

where DIV denotes the divergence operator computed in the material configuration, $\boldsymbol{P}$ represents the first Piola–Kirchhoff stress tensor, $\boldsymbol{b}_0$ is a body force per unit undeformed volume, and the accompanying boundary conditions are given by

$$\boldsymbol{P}\boldsymbol{N} = \bar{\boldsymbol{t}} \quad \text{on} \quad \partial\Omega_0^t; \tag{2.4a}$$

$$\boldsymbol{\phi} = \bar{\boldsymbol{\phi}} \quad \text{on} \quad \partial\Omega_0^u, \tag{2.4b}$$

where $\bar{\boldsymbol{t}}$ denotes the prescribed traction over part of boundary $\partial\Omega_0^t$, and $\bar{\boldsymbol{\phi}}$ are prescribed positions over $\partial\Omega_0^u$, where $\partial\Omega_0^t$ and $\partial\Omega_0^u$ are two complementary subsets, that is, $\partial\Omega_0^t \cap \partial\Omega_0^u = \emptyset$ and $\partial\Omega_0^t \cup \partial\Omega_0^u = \partial\Omega_0$. In addition, conservation of angular momentum leads to the well-known symmetry condition $\boldsymbol{P}\boldsymbol{F}^T = \boldsymbol{F}\boldsymbol{P}^T$ [75].

In the absence of magnetic and time-dependent effects, the description of the EAP response is completed with Faraday's and Gauss' laws. Although, in general, the presence of electric fields in the surrounding media, that is, the vacuum, must be accounted for, in the case of EAPs this can be safely neglected due to its negligible influence.[6] With this in mind, Faraday's law and associated boundary conditions are expressed as

$$\boldsymbol{E}_0 = -\nabla_0\varphi \quad \text{in} \quad \Omega_0; \tag{2.5a}$$

$$\varphi = \bar{\varphi} \quad \text{on} \quad \partial\Omega_0^\varphi, \tag{2.5b}$$

and Gauss' law and associated boundary condition as

$$\text{DIV } \boldsymbol{D}_0 = \rho_0 \quad \text{in} \quad \Omega_0; \tag{2.6a}$$

$$\boldsymbol{D}_0 \cdot \boldsymbol{N} = -\omega_0 \quad \text{on} \quad \partial\Omega_0^\omega, \tag{2.6b}$$

where $\boldsymbol{E}_0$ and $\boldsymbol{D}_0$ are the Lagrangian electric field and Lagrangian electric displacement, respectively, φ is the electric potential subjected to prescribed value $\bar{\varphi}$ on the boundary $\partial\Omega_0^\varphi$, ρ_0 is the electric density charge per unit undeformed volume and ω_0 is the electric charge per unit undeformed area applied over part of boundary $\partial\Omega_0^\omega$, such that $\partial\Omega_0^\omega \cap \partial\Omega_0^\varphi = \emptyset$ and $\partial\Omega_0^\omega \cup \partial\Omega_0^\varphi = \partial\Omega_0$. To close the system of governing Eqs. (2.1) to (2.6b), constitutive equations describing the behaviour of the EAP need to be introduced, which are presented in the following section.

---

[5] In addition, throughout the paper, the symbol $(\cdot)$ indicates the scalar product or contraction of a single index $\boldsymbol{a} \cdot \boldsymbol{b} = a_i b_i$; the symbol $(:)$, double contraction of two indices $\boldsymbol{A} : \boldsymbol{B} = A_{ij}B_{ij}$; the symbol $(\times)$, the cross product between vectors $(\boldsymbol{a} \times \boldsymbol{b})_i = \mathcal{E}_{ijk}a_j b_k$; and the symbol $(\otimes)$, the outer or dyadic product $(\boldsymbol{a} \otimes \boldsymbol{b})_{ij} = a_i b_j$.

[6] The reader is referred to [57] for the consideration of the vacuum at a continuum level and [47,48] for its numerical implementation.

2.3. Constitutive equations: reversible electro-mechanics

In the present paper, we resort to reversible behaviour described by electro-hyperelasticity [45] and introduce an internal energy e per unit volume in Ω_0, typically defined in terms of the two-point deformation gradient tensor $\boldsymbol{F}$ and the Lagrangian electric displacement vector $\boldsymbol{D}_0$, that is, $e = e(\boldsymbol{F}, \boldsymbol{D}_0)$, where $e : \mathbb{R}^{3\times3} \times \mathbb{R}^3 \to \mathbb{R} \cup \{+\infty\}$. For simplicity, we write $e = e(\mathcal{U})$ with $\mathcal{U} = (\boldsymbol{F}, \boldsymbol{D}_0)$.

Following standard thermodynamic arguments, that is the so-called Coleman–Noll procedure [76], the first directional derivative of the internal energy with respect to variations $\delta\mathcal{U} = (\delta\boldsymbol{F}, \delta\boldsymbol{D}_0)$ gives the first Piola–Kirchhoff stress tensor $\boldsymbol{P}$ and the electric field $\boldsymbol{E}_0$ as work (dual) conjugates of $\boldsymbol{F}$ and $\boldsymbol{D}_0$ as

$$De[\delta\mathcal{U}] = \partial_{\mathcal{U}}e \bullet \delta\mathcal{U} = \boldsymbol{P} : \delta\boldsymbol{F} + \boldsymbol{E}_0 \cdot \delta\boldsymbol{D}_0, \tag{2.7}$$

with

$$\boldsymbol{P}(\mathcal{U}) = \partial_{\boldsymbol{F}}e(\mathcal{U}); \qquad \boldsymbol{E}_0(\mathcal{U}) = \partial_{\boldsymbol{D}_0}e(\mathcal{U}), \tag{2.8}$$

where $\partial_A e$ denotes the partial derivative of e with respect to the field A and $\bullet$ denotes a suitable inner (dual) product. Similarly, assuming sufficient smoothness of the internal energy e, the second directional derivative of the internal energy yields the Hessian operator $\mathbb{H}_e$, that is,

$$D^2 e[\delta\mathcal{U}; \Delta\mathcal{U}] = \delta\mathcal{U} \bullet \mathbb{H}_e \bullet \Delta\mathcal{U}. \tag{2.9}$$

where symbol Δ is used to denote linearisation. For the sake of material characterisation, it is convenient to rewrite the Hessian $\mathbb{H}_e$ in terms of a fourth order type of elasticity tensor $\mathcal{C}_e \in \mathbb{R}^{3\times3\times3\times3}$, a third order type of piezoelectric tensor $\mathcal{Q} \in \mathbb{R}^{3\times3\times3}$ and a second-order type of dielectric tensor $\boldsymbol{\theta} \in \mathbb{R}^{3\times3}$ defined as

$$D^2 e[\delta\mathcal{U}; \Delta\mathcal{U}] = [\delta\boldsymbol{F} : \delta\boldsymbol{D}_0\cdot]\,\mathbb{H}_e \begin{bmatrix} : \Delta\boldsymbol{F} \\ \Delta\boldsymbol{D}_0 \end{bmatrix}; \qquad \mathbb{H}_e = \begin{bmatrix} \mathcal{C}_e & \mathcal{Q}^T \\ \mathcal{Q} & \boldsymbol{\theta} \end{bmatrix}, \tag{2.10}$$

where

$$\mathcal{C}_e(\mathcal{U}) = \partial^2_{\boldsymbol{F}\boldsymbol{F}}e(\mathcal{U}); \qquad \mathcal{Q}(\mathcal{U}) = \partial^2_{\boldsymbol{D}_0\boldsymbol{F}}e(\mathcal{U}); \qquad \boldsymbol{\theta}(\mathcal{U}) = \partial^2_{\boldsymbol{D}_0\boldsymbol{D}_0}e(\mathcal{U}), \tag{2.11}$$

with $\left(\mathcal{Q}^T\right)_{jJI} = (\mathcal{Q})_{IjJ}$.

2.3.1. The Helmholtz's free energy density function

For completeness, it is possible to introduce an alternative Helmholtz's type of energy density $\Psi = \Psi(\mathcal{W})$ with $\mathcal{W} = (\boldsymbol{F}, \boldsymbol{E}_0)$, where $\Psi : \mathbb{R}^{3\times3} \times \mathbb{R}^3 \to \mathbb{R} \cup \{+\infty\}$, as

$$\Psi(\mathcal{W}) = -\sup_{\boldsymbol{D}_0}\{\boldsymbol{E}_0 \cdot \boldsymbol{D}_0 - e(\mathcal{U})\}, \tag{2.12}$$

via the use of a partial Legendre transform in (2.12)[7], where the first Piola–Kirchhoff stress tensor and the electric displacement can be alternatively defined as

$$\boldsymbol{P}(\mathcal{W}) = \partial_{\boldsymbol{F}}\Psi(\mathcal{W}) \qquad \boldsymbol{D}_0(\mathcal{W}) = -\partial_{\boldsymbol{E}_0}\Psi(\mathcal{W}). \tag{2.13}$$

Similarly to (2.9), the second directional derivative of the Helmholtz's free energy density gives rise to the Hessian operator $\mathbb{H}_\Psi$ of Ψ as

$$D^2\Psi[\delta\mathcal{W}; \Delta\mathcal{W}] = \delta\mathcal{W} \bullet \mathbb{H}_\Psi \bullet \Delta\mathcal{W}, \tag{2.14}$$

which can be re-expressed in terms of the elasticity tensor $\mathcal{C}_\Psi \in \mathbb{R}^{3\times3\times3\times3}$, the piezoelectric tensor $\mathcal{P} \in \mathbb{R}^{3\times3\times3}$ and the dielectric tensor $\boldsymbol{\epsilon} \in \mathbb{R}^{3\times3}$ defined as

$$D^2\Psi[\delta\mathcal{W}; \Delta\mathcal{W}] = [\delta\boldsymbol{F} : \delta\boldsymbol{E}_0\cdot]\,\mathbb{H}_\Psi \begin{bmatrix} : \Delta\boldsymbol{F} \\ \Delta\boldsymbol{E}_0 \end{bmatrix}; \qquad \mathbb{H}_\Psi = \begin{bmatrix} \mathcal{C}_\Psi & -\mathcal{P}^T \\ -\mathcal{P} & -\boldsymbol{\epsilon} \end{bmatrix}, \tag{2.15}$$

where

$$\mathcal{C}_\Psi(\mathcal{W}) = \partial^2_{\boldsymbol{F}\boldsymbol{F}}\Psi(\mathcal{W}); \qquad \mathcal{P}(\mathcal{W}) = -\partial^2_{\boldsymbol{E}_0\boldsymbol{F}}\Psi(\mathcal{W}); \qquad \boldsymbol{\epsilon}(\mathcal{W}) = -\partial^2_{\boldsymbol{E}_0\boldsymbol{E}_0}\Psi(\mathcal{W}), \tag{2.16}$$

---

[7] A sufficient condition for the existence of the Helmholtz's energy density (2.12) is the convexity of the internal energy density e with respect to the field $\boldsymbol{D}_0$.

with $\left(\boldsymbol{\mathcal{P}}^T\right)_{jJI} = (\boldsymbol{\mathcal{P}})_{IjJ}$. It is possible [60] to relate the components of the Hessian operators of Ψ (2.11) and e (2.16) as

$$\boldsymbol{\epsilon} = \boldsymbol{\theta}^{-1}; \qquad \boldsymbol{\mathcal{P}}^T = -\boldsymbol{\mathcal{Q}} \cdot \boldsymbol{\epsilon}; \qquad \boldsymbol{\mathcal{C}}_\Psi = \boldsymbol{\mathcal{C}}_e + \boldsymbol{\mathcal{Q}}^T \cdot \boldsymbol{\mathcal{P}}, \tag{2.17}$$

where the inner product $\cdot$ above indicates contraction of the indices placed immediately before and after it.

2.4. Variational principles in reversible electro-mechanics

The solution of the boundary value problem defined by the governing Eqs. (2.1) to (2.6b), in conjunction with a suitable definition of the internal energy density e or Helmholtz's free energy density Ψ, is typically solved based on the direct methods of the calculus of variations. With that in mind, the **_first variational principle_** can be introduced as

$$(\boldsymbol{\phi}^*, \boldsymbol{D}_0^*) = \arg \inf_{\mathcal{A}_{\Pi_e}} \Pi_e (\boldsymbol{\phi}, \boldsymbol{D}_0), \tag{2.18}$$

where

$$\Pi_e (\boldsymbol{\phi}, \boldsymbol{D}_0) = \int_{\Omega_0} e (\boldsymbol{F}, \boldsymbol{D}_0) \, dV - \Pi_{\text{ext}}^m (\boldsymbol{\phi}), \tag{2.19}$$

$\Pi_{\text{ext}}^m(\boldsymbol{\phi})$ representing the external work done by the mechanical actions, defined as

$$\Pi_{\text{ext}}^m (\boldsymbol{\phi}) = \int_{\Omega_0} \boldsymbol{b}_0 \cdot \boldsymbol{\phi} \, dV + \int_{\partial \Omega_0^t} \bar{\boldsymbol{t}} \cdot \boldsymbol{\phi} \, dA, \tag{2.20}$$

and with the functional space $\mathcal{A}_{\Pi_e}$ given by

$$\mathcal{A}_{\Pi_e} = \left\{ \boldsymbol{\phi} \in \mathcal{G}_{\boldsymbol{\phi}}(\Omega_0; \mathbb{R}^3), \, \boldsymbol{D}_0 \in \mathcal{G}_{\boldsymbol{D}_0}(\Omega_0; \mathbb{R}^3); \ \text{s.t.} \ (2.4b), (2.6a), (2.6b) \right\}. \tag{2.21}$$

with $\mathcal{G}_{\boldsymbol{\phi}}, \mathcal{G}_{\boldsymbol{D}_0}$ suitable functional spaces to be defined. The use of the asterisk $(\cdot)^*$ in (2.18) denotes the solution (minimiser) of the variational principle. As it is well-known, for the existence of minimisers of the above variational problem, some mathematical restrictions must be imposed on $\mathcal{A}_{\Pi_e}$ and on the form that the internal energy density e must adopt [56,62], which will be the focus of the following section.

From the computational standpoint, it is convenient to resort to an alternative variational principle in order to by-pass the strong imposition of conditions (2.6) and allow the possibility of imposing boundary conditions directly on the electric potential (i.e. via electrodes attached to the EAP). Indeed, after the introduction of the electric potential φ (which can be understood as a Lagrange multiplier for the weak enforcement of Gauss' law (2.6), see [57,77] for more details), the **_second variational principle_** emerges as

$$(\boldsymbol{\phi}^*, \varphi^*, \boldsymbol{D}_0^*) = \arg \inf_{\mathcal{A}_{\tilde{\Pi}_{e,\boldsymbol{\phi}}}} \inf_{\mathcal{A}_{\tilde{\Pi}_{e,\boldsymbol{D}_0}}} \sup_{\mathcal{A}_{\tilde{\Pi}_{e,\varphi}}} \tilde{\Pi}_e (\boldsymbol{\phi}, \varphi, \boldsymbol{D}_0), \tag{2.22}$$

where

$$\tilde{\Pi}_e (\boldsymbol{\phi}, \varphi, \boldsymbol{D}_0) = \int_{\Omega_0} e (\boldsymbol{F}, \boldsymbol{D}_0) \, dV + \int_{\Omega_0} \boldsymbol{D}_0 \cdot \nabla_0 \varphi \, dV - \Pi_{\text{ext}} (\boldsymbol{\phi}, \varphi), \tag{2.23}$$

where $\Pi_{\text{ext}}(\boldsymbol{\phi}, \varphi)$ represents the combined external work done by the mechanical and electrical actions, defined as

$$\Pi_{\text{ext}} (\boldsymbol{\phi}, \varphi) = \Pi_{\text{ext}}^m (\boldsymbol{\phi}) + \Pi_{\text{ext}}^e (\varphi); \qquad \Pi_{\text{ext}}^e (\varphi) = - \int_{\Omega_0} \rho_0 \varphi \, dV - \int_{\partial \Omega_0^t} \omega_0 \varphi \, dA, \tag{2.24}$$

and with

$$\begin{aligned}
\mathcal{A}_{\tilde{\Pi}_{e,\boldsymbol{\phi}}} &= \left\{ \boldsymbol{\phi} \in \tilde{\mathcal{G}}_{\boldsymbol{\phi}}(\Omega_0; \mathbb{R}^3); \ \text{s.t.} \ (2.4b) \right\}; \\
\mathcal{A}_{\tilde{\Pi}_{e,\boldsymbol{D}_0}} &= \left\{ \boldsymbol{D}_0 \in \tilde{\mathcal{G}}_{\boldsymbol{D}_0}(\Omega_0; \mathbb{R}^3) \right\}; \\
\mathcal{A}_{\tilde{\Pi}_{e,\varphi}} &= \left\{ \varphi \in \tilde{\mathcal{G}}_{\varphi}(\Omega_0; \mathbb{R}); \ \text{s.t.} \ (2.5b) \right\},
\end{aligned} \tag{2.25}$$

with $\tilde{\mathcal{G}}_{\boldsymbol{\phi}}, \tilde{\mathcal{G}}_{\boldsymbol{D}_0}, \tilde{\mathcal{G}}_{\varphi}$ suitable functional spaces to be defined. Furthermore, use of the Helmholtz's free energy density functional (2.12) in (2.22) leads to the ***third variational principle*** as follows,

$$(\boldsymbol{\phi}^*, \varphi^*) = \arg \inf_{\mathcal{A}_{\Psi_{\boldsymbol{\phi}}}} \sup_{\mathcal{A}_{\Psi_{\varphi}}} \Pi_{\Psi}(\boldsymbol{\phi}, \varphi), \tag{2.26}$$

where

$$\Pi_{\Psi}(\boldsymbol{\phi}, \varphi) = \int_{\Omega_0} \Psi(\boldsymbol{F}, \boldsymbol{E}_0) \, dV - \Pi_{\text{ext}}(\boldsymbol{\phi}, \varphi), \tag{2.27}$$

where $\mathcal{A}_{\Psi_{\boldsymbol{\phi}}}$ and $\mathcal{A}_{\Psi_{\varphi}}$ are suitably adapted functional spaces analogous to their counterparts $\mathcal{A}_{\tilde{\Pi}_{e,\boldsymbol{\phi}}}$ and $\mathcal{A}_{\tilde{\Pi}_{e,\varphi}}$ in (2.25). The latter variational principle is typically preferred for numerical simulations due to its compact form and reduced number of degrees of freedom, described solely in terms of the mapping ϕ^* and the electrical potential φ^*.

3. Polyconvexity in electromechanics

To ensure the existence of solutions of the above variational principles Π_e (2.18), $\tilde{\Pi}_e$ (2.22) or Π_{Ψ} (2.26), the energy density e must fulfil certain mathematical requirements. In particular, we require, that the energy functionals are lower semicontinuous in a suitable topology. This relates to the convexity properties of the integrands. Prior to introducing the notion of polyconvexity in the context of electromechanics, the section starts by introducing some alternative mathematical restrictions (the reader is referred to the excellent monograph [70] for an in-depth discussion in the context of mechanics). The section continues by introducing the requirement of polyconvexity and its most relevant implications, namely, the existence of minimisers and the assurance of material stability.

3.1. Some notions on generalised convexity conditions

One of the simplest conditions is that of ***convexity*** of $e(\mathcal{U})$, that is

$$e(\lambda \mathcal{U}_1 + (1 - \lambda)\mathcal{U}_2) \leq \lambda e(\mathcal{U}_1) + (1 - \lambda)e(\mathcal{U}_2); \quad \forall \mathcal{U}_1, \mathcal{U}_2; \quad \lambda \in [0, 1], \tag{3.1}$$

which for functions with first order differentiability can be alternatively written as

$$e(\mathcal{U} + \delta\mathcal{U}) - e(\mathcal{U}) - De(\mathcal{U})[\delta\mathcal{U}] \geq 0; \qquad \forall \mathcal{U}, \delta\mathcal{U}, \tag{3.2}$$

and for functions with second order differentiability (in terms of the Hessian $[\mathbb{H}_e]$) as

$$D^2 e(\mathcal{U})[\delta\mathcal{U}; \delta\mathcal{U}] = \delta\mathcal{U} \bullet [\mathbb{H}_e] \bullet \delta\mathcal{U} \geq 0; \qquad \forall \mathcal{U}, \delta\mathcal{U}, \tag{3.3}$$

which requires (refer to (2.10), (2.11)) positive semi-definiteness of $\mathcal{C}_e$ and $\boldsymbol{\theta}$, independently, and further restrictions on the form that the third-order tensor $\mathcal{Q}$ can adopt. However, convexity away from the origin (i.e. $\boldsymbol{F} \approx \boldsymbol{I}$ and $\boldsymbol{D}_0 \approx \boldsymbol{0}$) is not a suitable physical restriction as it precludes the realistic behaviour of materials such as buckling in the purely mechanical context, as well as the possibility of voltage-induced buckling, inherent to soft dielectric materials [78]. An alternative mathematical restriction is that of $\mathcal{A}$-quasiconvexity of e [79]. Unfortunately, $\mathcal{A}$-quasiconvexity is a nonlocal condition that is very difficult, even impossible, to be verified.

A necessary restriction implied by $\mathcal{A}$-quasiconvexity is that of ***generalised rank-one convexity*** of e. A generalised rank-one convex energy density verifies

$$e(\lambda \mathcal{U} + (1 - \lambda)\tilde{\mathcal{U}}) \leq \lambda e(\mathcal{U}) + (1 - \lambda)e(\tilde{\mathcal{U}}); \quad \forall \mathcal{U}; \quad \lambda \in [0, 1], \tag{3.4}$$

and with $\tilde{\mathcal{U}} = \mathcal{U} + \delta\mathcal{U}$ and $\delta\mathcal{U} = (\boldsymbol{u} \otimes \boldsymbol{V}, \boldsymbol{V}_{\perp})$, where $\boldsymbol{V} \cdot \boldsymbol{V}_{\perp} = 0$ and with $\boldsymbol{u}, \boldsymbol{V}$ and $\boldsymbol{V}_{\perp}$ any arbitrary vectors. For the case of energies with first order differentiability, generalised rank-one convexity can alternatively be written as

$$e(\mathcal{U} + \delta\mathcal{U}) - e(\mathcal{U}) - De(\mathcal{U})[\delta\mathcal{U}] \geq 0; \qquad \delta\mathcal{U} = (\boldsymbol{u} \otimes \boldsymbol{V}, \boldsymbol{V}_{\perp}); \qquad \forall \mathcal{U}, \boldsymbol{u}, \boldsymbol{V}, \boldsymbol{V}_{\perp}, \tag{3.5}$$

and for energies with second order differentiability,

$$D^2 e(\mathcal{U})[\delta\mathcal{U}; \delta\mathcal{U}] = \delta\mathcal{U} \bullet \mathbb{H}_e \bullet \delta\mathcal{U} \geq 0; \qquad \delta\mathcal{U} = (\boldsymbol{u} \otimes \boldsymbol{V}, \boldsymbol{V}_{\perp}); \qquad \forall \mathcal{U}, \boldsymbol{u}, \boldsymbol{V}, \boldsymbol{V}_{\perp}. \tag{3.6}$$

The generalised rank-one convexity restriction in its form (3.5) plays a key role in the suitable definition of jump conditions across a travelling interface defined by a normal vector $\boldsymbol{V}$ moving with speed c (i.e. singular surface [80]). Analogously, condition (3.6) is referred to as the Legendre–Hadamard condition or ***ellipticity*** of e, linked to the propagation of travelling plane wave within the material defined by a vector $\boldsymbol{V}$ and speed c. These two aspects will be presented in the following two subsections.

3.1.1. Generalised rank-one convexity conditions and jump conditions

Consider a travelling discontinuity within an EAP, moving at speed c and defined by a normal vector $\boldsymbol{V}$ separating states $(\bullet)^a$ and $(\bullet)^b$, where $[\![\bullet]\!] = (\bullet)^a - (\bullet)^b$ denotes the jump across the interface and $(\bullet)^{\mathrm{Av}} = 1/2((\bullet)^a + (\bullet)^b)$ the average state. Following [58], the jump or Rankine–Hugoniot conditions for the combined set of Cauchy-Maxwell (electro-magneto-mechanical) equations are given by

$$-c[\![\boldsymbol{F}]\!] = [\![\boldsymbol{v}]\!] \otimes \boldsymbol{V}; \tag{3.7a}$$

$$-c\rho_R[\![\boldsymbol{v}]\!] = [\![\boldsymbol{P}]\!]\boldsymbol{V}; \tag{3.7b}$$

$$-c[\![\boldsymbol{B}_0]\!] = [\![\boldsymbol{E}_0]\!] \times \boldsymbol{V}; \tag{3.7c}$$

$$c[\![\boldsymbol{D}_0]\!] = [\![\boldsymbol{H}_0]\!] \times \boldsymbol{V}; \tag{3.7d}$$

$$-c[\![e + 1/2\rho_R\boldsymbol{v} \cdot \boldsymbol{v}]\!] = [\![\boldsymbol{v} \cdot \boldsymbol{P}]\!] \cdot \boldsymbol{V} - [\![\boldsymbol{E}_0 \times \boldsymbol{H}_0]\!] \cdot \boldsymbol{V}, \tag{3.7e}$$

where, in addition to previously defined fields, ρ_R, $\boldsymbol{v}$, $\boldsymbol{B}_0$ and $\boldsymbol{H}_0$ denote the density of the material per unit undeformed volume, the velocity, the magnetic induction vector and the magnetic field, respectively. Substitution of (3.7a)–(3.7d) into (3.7e) renders

$$[\![e]\!] = \boldsymbol{P}^{\mathrm{Av}} : [\![\boldsymbol{F}]\!] + \boldsymbol{E}_0^{\mathrm{Av}} \cdot [\![\boldsymbol{D}_0]\!] + \boldsymbol{H}_0^{\mathrm{Av}} \cdot [\![\boldsymbol{B}_0]\!], \tag{3.8}$$

which, by re-defining $(\bullet)^{\mathrm{Av}} = (\bullet)^a + [\![\bullet]\!]/2$ and removing the upper index $(\bullet)^a$ for simplicity, can be rewritten as

$$[\![e]\!] - \boldsymbol{P} : [\![\boldsymbol{F}]\!] - \boldsymbol{E}_0 \cdot [\![\boldsymbol{D}_0]\!] - \boldsymbol{H}_0 \cdot [\![\boldsymbol{B}_0]\!] = [\![\boldsymbol{P}]\!] : [\![\boldsymbol{F}]\!] + [\![\boldsymbol{E}_0]\!] \cdot [\![\boldsymbol{D}_0]\!] + [\![\boldsymbol{H}_0]\!] \cdot [\![\boldsymbol{B}_0]\!]. \tag{3.9}$$

For the case when magnetic effects are neglected (i.e. $[\![\boldsymbol{B}_0]\!] \approx \boldsymbol{0}$) the last term on both sides of Eq. (3.9) can be neglected. Moreover, notice that the term $[\![\boldsymbol{E}_0]\!] \cdot [\![\boldsymbol{D}_0]\!] \approx 0$ as $\boldsymbol{E}_0$ can only jump tangentially across the discontinuity (refer to (3.7c)) whilst $\boldsymbol{D}_0$ can only jump along $\boldsymbol{V}$ (refer to (3.7d)), that is, $[\![\boldsymbol{D}_0]\!] = \boldsymbol{V}_\perp$, $\boldsymbol{V} \cdot \boldsymbol{V}_\perp = 0$. Thus, we arrive at the simpler equation

$$[\![e]\!] - \boldsymbol{P} : [\![\boldsymbol{F}]\!] - \boldsymbol{E}_0 \cdot \boldsymbol{V}_\perp = [\![\boldsymbol{P}]\!] : [\![\boldsymbol{F}]\!]. \tag{3.10}$$

Redefining $-[\![\boldsymbol{v}]\!]/c = \boldsymbol{u}$, that is $[\![\boldsymbol{F}]\!] = \boldsymbol{u} \otimes \boldsymbol{V}$, and making use of (3.7a) and (3.7b), it is straightforward to show that $[\![\boldsymbol{P}]\!] : [\![\boldsymbol{F}]\!] = \rho_R c^2 \boldsymbol{u} \cdot \boldsymbol{u}$, which finally gives

$$[\![e]\!] - \boldsymbol{P} : (\boldsymbol{u} \otimes \boldsymbol{V}) - \boldsymbol{E}_0 \cdot \boldsymbol{V}_\perp = \rho_R c^2 \boldsymbol{u} \cdot \boldsymbol{u} \geq 0, \tag{3.11}$$

which can be equivalently written as

$$e(\boldsymbol{F} + \boldsymbol{u} \otimes \boldsymbol{V}, \boldsymbol{D}_0 + \boldsymbol{V}_\perp) - e(\boldsymbol{F}, \boldsymbol{D}_0) - \partial_{\boldsymbol{F}}e(\boldsymbol{F}, \boldsymbol{D}_0) : (\boldsymbol{u} \otimes \boldsymbol{V}) - \partial_{\boldsymbol{D}_0}e(\boldsymbol{F}, \boldsymbol{D}_0) \cdot \boldsymbol{V}_\perp \geq 0. \tag{3.12}$$

Notice that above inequality (3.12) holds for an energy density e defined as generalised rank-one convexity (refer to Eq. (3.5)).

3.1.2. Ellipticity and Legendre-Hadamard condition

Condition (3.6) is referred to as the Legendre–Hadamard condition or ellipticity of e and is related to the propagation of travelling plane waves[8] within the material defined by a vector $\boldsymbol{V}$ and speed c. Notice that the above expression (3.6) is a generalisation of the concept of ellipticity from elasticity to the more general case of electro-elasticity, which can be easily verified by neglecting the piezoelectric and dielectric components of the Hessian operator, that is

$$(\boldsymbol{u} \otimes \boldsymbol{V}) : \mathcal{C}_e(\mathcal{U}) : (\boldsymbol{u} \otimes \boldsymbol{V}) \geq 0; \qquad \forall \mathcal{U}, \boldsymbol{u}, \boldsymbol{V}. \tag{3.13}$$

Similarly, particularising for $\boldsymbol{u} = \boldsymbol{0}$ in either (3.5) or (3.6), it reduces to the condition of convexity with respect to $\boldsymbol{D}_0$. This condition is crucial in order to guarantee the existence of the Helmholtz's free energy density function (2.12) and thus that of the variational principle Π_Ψ (2.26).

The derivation of the above Legendre–Hadamard condition (3.6) has its roots in the study of the hyperbolicity (or stability in the quasi-static case) of the system of the generalised Cauchy-Maxwell equations [58] in order to

---

[8] This concept is also strongly related to that of the propagation of **acceleration waves** within a discontinuity defined by a normal vector $\boldsymbol{V}$ with speed c.

ensure the existence of real wave speeds propagating throughout the domain. Crucially, the *ab initio* existence of real wave speeds for the specific system of governing Eqs. (2.1) to (2.6b) (i.e. magnetic and time-dependent effects are neglected in the Maxwell equations) can be monitored via the study of the so-called electro-mechanical acoustic tensor $\boldsymbol{Q}$ defined as

$$\boldsymbol{Q} = \mathcal{C}_{e,VV} + \boldsymbol{\mathcal{Q}}_V^T \boldsymbol{\theta}^{-1} \left[\frac{\boldsymbol{V} \otimes \boldsymbol{\theta}^{-1} \boldsymbol{V}}{\boldsymbol{V} \cdot \boldsymbol{\theta}^{-1} \boldsymbol{V}} - \boldsymbol{I} \right] \boldsymbol{\mathcal{Q}}_V, \tag{3.14}$$

where

$$\left[\mathcal{C}_{e,VV} \right]_{ij} = \mathcal{C}_{e,iIjJ} V_I V_J, \qquad [\boldsymbol{\mathcal{Q}}_V]_{Ij} = \mathcal{Q}_{IjJ} V_J, \qquad [\boldsymbol{I}]_{IJ} = \delta_{IJ}. \tag{3.15}$$

Specifically, the eigenvalues of the acoustic tensor $\boldsymbol{Q}$ are proportional to the squared of the volumetric and shear wave speeds of the electroactive material. Hence, the above tensor $\boldsymbol{Q}$ can be used as a suitable localisation measure for the onset of material instabilities by ensuring that the wave speeds are kept real throughout the entire electro-deformation process. This can be achieved by ensuring that

$$\boldsymbol{u} \cdot \boldsymbol{Q}(\boldsymbol{\mathcal{U}})\boldsymbol{u} \geq 0; \qquad \forall \boldsymbol{\mathcal{U}}, \boldsymbol{u}, \boldsymbol{V} \tag{3.16}$$

or alternatively written as

$$(\boldsymbol{u} \otimes \boldsymbol{V}) : \left[\mathcal{C}_e + \underbrace{\boldsymbol{\mathcal{Q}}^T \boldsymbol{\theta}^{-1} \left[\frac{\boldsymbol{V} \otimes \boldsymbol{\theta}^{-1} \boldsymbol{V}}{\boldsymbol{V} \cdot \boldsymbol{\theta}^{-1} \boldsymbol{V}} - \boldsymbol{I} \right] \boldsymbol{\mathcal{Q}}}_{\mathcal{C}_e'} \right] : (\boldsymbol{u} \otimes \boldsymbol{V}) \geq 0; \qquad \forall \boldsymbol{u}, \boldsymbol{V}. \tag{3.17}$$

Comparison of (3.17) against (3.13) permits to identify the modification of the traditional ellipticity condition in elasticity with that of electro-elasticity via the additional contribution $\mathcal{C}_e'$, playing a key role in the modification of the dilatational and shear wave speeds from those of simple elasticity. The reader is referred to [58] for a comprehensive derivation of the acoustic tensor for the combined electro-magneto-mechanical case. A more compact derivation for the specific electro-mechanical case of interest in this paper is included in Appendix A.1.

3.2. $\mathcal{A}$-polyconvexity

Motivated by considerations of material stability (i.e. existence of real wave speeds) first and existence of minimisers subsequently, Gil and Ortigosa in [57,58,60,81] and Šilhavý in [62] extended the concept of polyconvexity [56,63,82–84] from elasticity to electro-magneto-elasticity and proposed a new convexity restriction on the form that the internal energy can adopt, that is, $\mathcal{A}$-**polyconvexity** of e. Following [62], the internal energy $e : \mathbb{R}^{3\times 3} \times \mathbb{R}^3 \to \mathbb{R} \cup \{+\infty\}$ is defined as $\mathcal{A}$-polyconvex if there exists a convex and lower semicontinuous function $W : \mathbb{R}^{3\times 3} \times \mathbb{R}^{3\times 3} \times \mathbb{R} \times \mathbb{R}^3 \times \mathbb{R}^3 \to \mathbb{R} \cup \{+\infty\}$ (in general non-unique) defined as

$$e(\boldsymbol{\mathcal{U}}) = W(\boldsymbol{\mathcal{V}}); \quad \boldsymbol{\mathcal{V}} = (\boldsymbol{F}, \boldsymbol{H}, J, \boldsymbol{D}_0, \boldsymbol{d}); \quad \boldsymbol{d} = \boldsymbol{F}\boldsymbol{D}_0. \tag{3.18}$$

Notice that convexity of $W(\boldsymbol{\mathcal{V}})$ implies that

$$W(\lambda \boldsymbol{\mathcal{V}}_1 + (1-\lambda)\boldsymbol{\mathcal{V}}_2) \leq \lambda W(\boldsymbol{\mathcal{V}}_1) + (1-\lambda)W(\boldsymbol{\mathcal{V}}_2); \quad \forall \boldsymbol{\mathcal{V}}_1, \boldsymbol{\mathcal{V}}_2; \quad \lambda \in [0,1]. \tag{3.19}$$

which for functions with sufficient differentiability, can be alternatively written as

$$W(\boldsymbol{\mathcal{V}} + \delta\boldsymbol{\mathcal{V}}) - W(\boldsymbol{\mathcal{V}}) - DW(\boldsymbol{\mathcal{V}})[\delta\boldsymbol{\mathcal{V}}] \geq 0; \qquad \forall \boldsymbol{\mathcal{V}}, \delta\boldsymbol{\mathcal{V}}, \tag{3.20}$$

or even in terms of the Hessian operator $[\mathbb{H}_W]$ as

$$D^2 W(\boldsymbol{\mathcal{V}})[\delta\boldsymbol{\mathcal{V}}; \Delta\boldsymbol{\mathcal{V}}] = \delta\boldsymbol{\mathcal{V}} \bullet [\mathbb{H}_W] \bullet \Delta\boldsymbol{\mathcal{V}} \geq 0; \qquad \forall \boldsymbol{\mathcal{V}}, \delta\boldsymbol{\mathcal{V}}, \Delta\boldsymbol{\mathcal{V}}. \tag{3.21}$$

As presented by Šilhavý in [62], $\mathcal{A}$-polyconvexity in conjunction with suitable growth conditions, ensures the existence of minimisers in nonlinear electro-magneto-elasticity, which is briefly recalled in the following section.

3.3. $\mathcal{A}$-polyconvexity and existence of minimisers

The extended set of arguments in W, that is $\mathcal{V}$, has a special property; namely, they are weakly sequentially continuous [85].

Proposition 3.1. *Let $\Omega_0 \subset \mathbb{R}^3$ be a bounded Lipschitz domain. Let $(\boldsymbol{\phi}_k)_{k \in N} \subset W^{1,p}(\Omega_0; \mathbb{R}^3)$ for some $p > 3$ and let $\boldsymbol{\phi}_k \to \boldsymbol{\phi}$ weakly for some $\boldsymbol{\phi} \in W^{1,p}(\Omega_0; \mathbb{R}^3)$. Then*

$$\text{Cof}\,\nabla_0\boldsymbol{\phi}_k \to \text{Cof}\,\nabla_0\boldsymbol{\phi} \;\; weakly \; in \; L^{p/2}(\Omega_0; \mathbb{R}^{3\times3})\,, \tag{3.22a}$$

$$\det\nabla_0\boldsymbol{\phi}_k \to \det\nabla_0\boldsymbol{\phi} \;\; weakly \; in \; L^{p/3}(\Omega_0)\,. \tag{3.22b}$$

Proposition 3.2. *Let $\Omega_0 \subset \mathbb{R}^3$ be a bounded Lipschitz domain. Let $\boldsymbol{\phi}_k \to \boldsymbol{\phi}$ weakly in $W^{1,p}(\Omega_0; \mathbb{R}^3)$ for some $1 < p < +\infty$ and let $\boldsymbol{D}_{0,k} \to \boldsymbol{D}_0$ weakly in $L^q(\Omega_0; \mathbb{R}^3)$ where $1/q + 1/p < 1$ and $\text{DIV}\,\boldsymbol{D}_{0,k} = \text{DIV}\,\boldsymbol{D}_0 = \rho_0$ for every $k \in N$ and for some $\rho_0 \in W^{-1,1}(\Omega)$. Then $\boldsymbol{d}_k = \boldsymbol{F}_k\boldsymbol{D}_{0,k} \to \boldsymbol{d} = \boldsymbol{F}\boldsymbol{D}_0$ weakly in $L^1(\Omega_0; \mathbb{R}^3)$, where $\boldsymbol{F}_k = \nabla\boldsymbol{\phi}_k$ and $\boldsymbol{F} = \nabla\boldsymbol{\phi}$.*

Referring now to the variational principle Π_e previously presented in (2.19), it is now possible to introduce the following theorem of existence of minimisers. Indeed,

Theorem 3.1. *Let $\Omega_0 \subset \mathbb{R}^3$ be a bounded Lipschitz domain. Let $p > 2$, $p_c \geq p/(p-1)$, $r > 1$, and $q > p/(p-1)$, and let the following **growth conditions** be satisfied for some constant $C > 0$.*

$$e(\mathcal{U}) \begin{cases} \geq C(\|\boldsymbol{F}\|^p + \|\boldsymbol{H}\|^{p_c} + J^r + \|\boldsymbol{D}_0\|^q) \; if \; J > 0\,, \\ = +\infty \; otherwise. \end{cases} \tag{3.23}$$

*Moreover, assume that e is $\mathcal{A}$-**polyconvex**, i.e., that (3.18) holds for some convex and lower semicontinuous function $W : \mathbb{R}^{3\times3} \times \mathbb{R}^{3\times3} \times \mathbb{R} \times \mathbb{R}^3 \times \mathbb{R}^3 \to \mathbb{R} \cup \{+\infty\}$ and that*

$$e(\mathcal{U}) = W(\mathcal{V}) \to +\infty \; if \; J \to 0. \tag{3.24}$$

Let

$$\mathcal{A} = \{\boldsymbol{\phi} \in W^{1,p}(\Omega_0; \mathbb{R}^3), \quad \boldsymbol{D}_0 \in L^q(\Omega_0; \mathbb{R}^3);$$
$$s.t. \; \boldsymbol{H} \in L^{p_c}(\Omega_0; \mathbb{R}^{3\times3}); \quad J \in L^r(\Omega_0)\,, \; J > 0 \; a.e.;$$
$$s.t. \; (2.4b), (2.6a), (2.6b)\}$$

*be non-empty and such that $\inf_{\mathcal{A}} \Pi_e < +\infty$. Then there is a **minimiser** of Π_e on $\mathcal{A}$.*

Proof. The proof follows the same lines as in [85]. If $(\boldsymbol{\phi}_k, (\boldsymbol{D}_0)_k) \subset W^{1,p}(\Omega_0; \mathbb{R}^3) \times L^q(\Omega_0; \mathbb{R}^3)$ is a minimising sequence then (3.23) and the Dirichlet boundary conditions ensure that this minimising sequence is bounded in $W^{1,p}(\Omega_0; \mathbb{R}^3) \times L^q(\Omega_0; \mathbb{R}^3)$. Therefore, it holds for a non-relabelled subsequence that $\boldsymbol{\phi}_k \to \boldsymbol{\phi}$ weakly and $(\boldsymbol{D}_0)_k \to \boldsymbol{D}_0$ weakly. Further, $\boldsymbol{F}_k(\boldsymbol{D}_0)_k \to \boldsymbol{F}(\boldsymbol{D}_0)$ weakly in $L^{pq/(p+q)}(\Omega; \mathbb{R}^3)$ due to Proposition 3.2. $\square$

3.4. $\mathcal{A}$-polyconvexity and material stability: extended set of work conjugates and the tangent operator

As presented in [57,58,60,81], the consideration of the function W (instead of its equivalent energetic expression e) permits the introduction of the set $\boldsymbol{\Sigma}_{\mathcal{V}}$ of work conjugate fields $\boldsymbol{\Sigma}_{\mathcal{V}} = (\boldsymbol{\Sigma}_F, \boldsymbol{\Sigma}_H, \Sigma_J, \boldsymbol{\Sigma}_{D_0}, \boldsymbol{\Sigma}_d)$ defined as

$$DW[\delta\mathcal{V}] = \boldsymbol{\Sigma}_{\mathcal{V}} \bullet \delta\mathcal{V}; \qquad \boldsymbol{\Sigma}_{\mathcal{V}}(\mathcal{V}) = \partial_{\mathcal{V}}W(\mathcal{V}). \tag{3.25}$$

Moreover, for the particular case when $\delta\mathcal{V} = D\mathcal{V}[\delta\mathcal{U}]$, comparing Eqs. (2.7) and (3.25) yields [57]

$$\boldsymbol{P} = \boldsymbol{\Sigma}_F + \boldsymbol{\Sigma}_H \times \boldsymbol{F} + \Sigma_J \boldsymbol{H} + \boldsymbol{\Sigma}_d \otimes \boldsymbol{D}_0; \qquad \boldsymbol{E}_0 = \boldsymbol{\Sigma}_{D_0} + \boldsymbol{F}^T\boldsymbol{\Sigma}_d, \tag{3.26}$$

which, for the case of a suitably defined convex energy function W, facilitates the evaluation of $\boldsymbol{P}$ and $\boldsymbol{E}_0$ in terms of the sets $\mathcal{V}$ and $\boldsymbol{\Sigma}_{\mathcal{V}}$. Assuming sufficient regularity of the function W, its second directional derivative yields the Hessian operator $\mathbb{H}_W$ as

$$D^2W[\delta\mathcal{V}; \Delta\mathcal{V}] = \delta\mathcal{V} \bullet \mathbb{H}_W \bullet \Delta\mathcal{V}, \tag{3.27}$$

By definition, $\mathcal{A}$-polyconvexity implies semi-positive definiteness of the Hessian operator $\mathbb{H}_W$ (refer to (3.21)). Moreover, as also shown in [57,58,60,81], the second directional derivative of the internal energy e (2.9) can be equivalently expressed in terms of its extended representation W as

$$D^2 e\,[\delta\mathcal{U};\,\Delta\mathcal{U}] = D^2 W[D\mathcal{V}[\delta\mathcal{U}];\,D\mathcal{V}[\Delta\mathcal{U}]] + (\boldsymbol{\Sigma_H} + \Sigma_J\boldsymbol{F}) : (\delta\boldsymbol{F}\times\delta\boldsymbol{F}) + 2\boldsymbol{\Sigma_d}\cdot\delta\boldsymbol{F}\,\delta\boldsymbol{D}_0, \tag{3.28}$$

where

$$D^2 W[D\mathcal{V}[\delta\mathcal{U}];\,D\mathcal{V}[\Delta\mathcal{U}]] = \mathbb{S}^T\mathbb{H}_W\mathbb{S}, \tag{3.29}$$

with $\mathbb{S}$ defined as

$$\mathbb{S} = \begin{bmatrix} : \delta\boldsymbol{F} \\ : (\delta\boldsymbol{F}\times\boldsymbol{F}) \\ \delta\boldsymbol{F} : \boldsymbol{H} \\ \cdot\delta\boldsymbol{D}_0 \\ \cdot(\delta\boldsymbol{F}\boldsymbol{D}_0 + \boldsymbol{F}\delta\boldsymbol{D}_0) \end{bmatrix}. \tag{3.30}$$

As presented in [60], it is possible to relate the components of the Hessian $\mathbb{H}_e$ in (2.9) to those of the Hessian $\mathbb{H}_W$ via appropriate algebraic transformations, which is advantageous for the case of energetic expressions defined in terms of W. Moreover, replacing $\delta\boldsymbol{F}$ and $\delta\boldsymbol{D}_0$ in (3.28) with $\delta\boldsymbol{F} = \boldsymbol{u}\otimes\boldsymbol{V}$ and $\delta\boldsymbol{D}_0 = \boldsymbol{V}_\perp$, respectively, and noticing that $De[\delta\mathcal{U}] = DW[D\mathcal{V}[\delta\mathcal{U}]]$, implies that Eq. (3.20) reduces to (3.5), which shows that $\mathcal{A}$-polyconvexity implies generalised rank-one convexity (in the more generic sense of electromechanics). Moreover, replacing $\delta\boldsymbol{F}$ and $\delta\boldsymbol{D}_0$ in (3.28) with $\delta\boldsymbol{F} = \boldsymbol{u}\otimes\boldsymbol{V}$ and $\delta\boldsymbol{D}_0 = \boldsymbol{V}_\perp$, respectively, permits to cancel the last two terms (also known as geometric terms) on the right-hand side of (3.28), and leads to

$$D^2 e[\boldsymbol{u}\otimes\boldsymbol{V},\,\boldsymbol{V}_\perp;\,\boldsymbol{u}\otimes\boldsymbol{V},\,\boldsymbol{V}_\perp] = \mathbb{S}^T\mathbb{H}_W\mathbb{S} \geq 0. \tag{3.31}$$

Relation (3.31) clearly illustrates that smooth $\mathcal{A}$-polyconvex internal energy functionals, characterised by a semi-positive definite Hessian operator $\mathbb{H}_W$, guarantee semi-positiveness of the left-hand side of Eq. (3.31), and hence the fulfilment of the ellipticity condition in (3.6).

4. Polyconvex transversely isotropic invariant-based electromechanics

In addition to the requirement of $\mathcal{A}$-polyconvexity (i.e. existence of minimisers and material stability), the internal energy density e must be defined satisfying additional requirements. The following subsection summarises them leading to an invariant-based representation of the energy density.

4.1. Invariant energy representation

Objectivity or frame invariance implies independence of the energy density with respect to arbitrary rotations $\boldsymbol{Q}$ of the spatial configuration, which can be formulated as

$$e(\boldsymbol{Q}\boldsymbol{F},\,\boldsymbol{D}_0) = e(\boldsymbol{F},\,\boldsymbol{D}_0);\qquad \forall\,\boldsymbol{Q}\in\mathrm{SO}(3), \tag{4.1}$$

with SO(3) the special (proper) orthogonal group [86]. Notice that in above objectivity requirement, the rotation tensor $\boldsymbol{Q}$ is only applied to the two-point tensor $\boldsymbol{F}$ and not to the Lagrangian vector $\boldsymbol{D}_0$. As it is well-known, the requirement of objectivity implies that the internal energy e must be expressible in terms of an objective set of arguments as $e(\boldsymbol{F},\,\boldsymbol{D}_0) = \tilde{e}(\boldsymbol{C},\,\boldsymbol{D}_0)$, where $\boldsymbol{C} = \boldsymbol{F}^T\boldsymbol{F}$ denotes the right Cauchy–Green strain tensor and with e and $\tilde{e}$ denoting alternative functional representations of the same internal energy density.

In addition, for the case of transverse isotropy[9] characterised by a material unit vector $\boldsymbol{M}$, the energy must be independent with respect to rotations/reflections $\boldsymbol{Q}\in\mathcal{G_m}\subset\mathrm{O}(3)$ of the material configuration, where $\mathcal{G_m}$ denotes the corresponding symmetry group and O(3) the full orthogonal group. The associated symmetry transformation is formulated as

$$\tilde{e}(\boldsymbol{Q}\boldsymbol{C}\,\boldsymbol{Q}^T,\,\boldsymbol{Q}\boldsymbol{D}_0) = \tilde{e}(\boldsymbol{C},\,\boldsymbol{D}_0);\qquad \forall\,\boldsymbol{Q}\in\mathcal{G_m}\subset\mathrm{O}(3). \tag{4.2}$$

---

[9] Or any other kind of anisotropy characterised by a possibly more complex crystal symmetry structure.

As stated e.g. in [73], there exist five types of transverse isotropy. In this work, we restrict ourselves to those that affect most EAPs of interest, that is, the symmetry $\mathcal{D}_{\infty h}$, which corresponds to the usual definition of transverse isotropy (e.g. applicable to electro-active polymers), and the symmetry $\mathcal{C}_{\infty}$, the so-called rotational symmetry (e.g. applicable to electro-active materials exhibiting piezoelectric effects). Please refer to [71–73] for further details regarding the various types of transverse isotropy. Moreover, these two symmetry groups can be characterised by appropriate *structural tensors* which encapsulate the symmetry attributes of their corresponding groups, which in this case are given by the second-order tensor $\boldsymbol{M} \otimes \boldsymbol{M}$ (for $\mathcal{D}_{\infty h}$) and the first-order tensor (vector) $\boldsymbol{M}$ (for $\mathcal{C}_{\infty}$).

By making use of the *isotropicisation theorem* [72], it is now possible to re-express above anisotropic restriction (4.2) for every $\boldsymbol{Q} \in \mathrm{O}(3)$ as

$$\bar{e}_{\mathcal{D}_{\infty h}}(\boldsymbol{Q}\boldsymbol{C}\boldsymbol{Q}^T, \boldsymbol{Q}(\boldsymbol{D}_0 \otimes \boldsymbol{D}_0)\boldsymbol{Q}^T, \boldsymbol{Q}(\boldsymbol{M} \otimes \boldsymbol{M})\boldsymbol{Q}^T) = \bar{e}_{\mathcal{D}_{\infty h}}(\boldsymbol{C}, \boldsymbol{D}_0 \otimes \boldsymbol{D}_0, \boldsymbol{M} \otimes \boldsymbol{M}) \tag{4.3a}$$

$$\bar{e}_{\mathcal{C}_{\infty}}(\boldsymbol{Q}\boldsymbol{C}\boldsymbol{Q}^T, \boldsymbol{Q}\boldsymbol{D}_0, \boldsymbol{Q}\boldsymbol{M}) = \bar{e}_{\mathcal{C}_{\infty}}(\boldsymbol{C}, \boldsymbol{D}_0, \boldsymbol{M}) \tag{4.3b}$$

where $\bar{e}_{\mathcal{D}_{\infty h}}$ and $\bar{e}_{\mathcal{C}_{\infty}}$ represent alternative isotropic functional representations of the internal energy density e particularised for their corresponding transverse isotropy groups $\mathcal{D}_{\infty h}$ and $\mathcal{C}_{\infty}$, respectively. It is now straightforward to obtain an irreducible list of isotropic invariants (a so-called *integrity basis*) for the characterisation of above energy densities $\bar{e}_{\mathcal{D}_{\infty h}}$ and $\bar{e}_{\mathcal{C}_{\infty}}$. For the case of $\bar{e}_{\mathcal{D}_{\infty h}}$ (refer to Table 12 in [72]), we obtain

$$
\begin{aligned}
\text{isotropic elasticity:} \quad & \mathrm{tr}[\boldsymbol{C}]; \ \mathrm{tr}[\boldsymbol{C}^2]; \ \mathrm{tr}[\boldsymbol{C}^3]; \\
+\text{isotropic electro:} \quad & \mathrm{tr}[\boldsymbol{D}_0 \otimes \boldsymbol{D}_0]; \ \mathrm{tr}[\boldsymbol{C}(\boldsymbol{D}_0 \otimes \boldsymbol{D}_0)]; \ \mathrm{tr}[\boldsymbol{C}^2(\boldsymbol{D}_0 \otimes \boldsymbol{D}_0)]; \\
+\text{transverse-isotropic elasticity:} \quad & \mathrm{tr}[\boldsymbol{C}(\boldsymbol{M} \otimes \boldsymbol{M})]; \ \mathrm{tr}[\boldsymbol{C}^2(\boldsymbol{M} \otimes \boldsymbol{M})]; \\
+\text{transverse-isotropic electro:} \quad & \mathrm{tr}[(\boldsymbol{D}_0 \otimes \boldsymbol{D}_0)(\boldsymbol{M} \otimes \boldsymbol{M})]; \ \mathrm{tr}[(\boldsymbol{D}_0 \otimes \boldsymbol{D}_0)\boldsymbol{C}(\boldsymbol{M} \otimes \boldsymbol{M})],
\end{aligned}
\tag{4.4}
$$

and for the case of $\bar{e}_{\mathcal{C}_{\infty}}$ (refer to Table 12 in [72]), we obtain[10]

$$
\begin{aligned}
\text{isotropic elasticity:} \quad & \mathrm{tr}[\boldsymbol{C}]; \ \mathrm{tr}[\boldsymbol{C}^2]; \ \mathrm{tr}[\boldsymbol{C}^3]; \\
+\text{isotropic electro:} \quad & \mathrm{tr}[\boldsymbol{D}_0 \otimes \boldsymbol{D}_0]; \ \mathrm{tr}[\boldsymbol{C}(\boldsymbol{D}_0 \otimes \boldsymbol{D}_0)]; \ \mathrm{tr}[\boldsymbol{C}^2(\boldsymbol{D}_0 \otimes \boldsymbol{D}_0)] \\
+\text{transverse-isotropic elasticity:} \quad & \mathrm{tr}[\boldsymbol{C}(\boldsymbol{M} \otimes \boldsymbol{M})]; \ \mathrm{tr}[\boldsymbol{C}^2(\boldsymbol{M} \otimes \boldsymbol{M})]; \\
+\text{transverse-isotropic electro:} \quad & \mathrm{tr}[\boldsymbol{D}_0 \otimes \boldsymbol{M}]; \ \mathrm{tr}[\boldsymbol{C}(\boldsymbol{D}_0 \otimes \boldsymbol{M})].
\end{aligned}
\tag{4.5}
$$

Notice that both integrity bases (4.4) and (4.5) are comprised of ten invariants, only differing in the expression of the two invariants responsible for the transversely isotropic electro-mechanic effect. It is now possible to re-express the above energy densities in terms of the invariants of the above integrity bases. Specifically, for the case of $\bar{e}_{\mathcal{D}_{\infty h}}$, it yields

$$\bar{e}_{\mathcal{D}_{\infty h}}(\boldsymbol{C}, \boldsymbol{D}_0 \otimes \boldsymbol{D}_0, \boldsymbol{M} \otimes \boldsymbol{M}) = \hat{e}_{\mathcal{D}_{\infty h}}(J_1, J_2, J_3, J_4, J_5, J_6, J_7, J_8, K_1^{\mathcal{D}_{\infty h}}, K_2^{\mathcal{D}_{\infty h}}), \tag{4.6}$$

where $J_i, \{i = 1 \ldots 8\}$ denote the following set of invariants

$$
\begin{aligned}
J_1 = \mathrm{tr}[\boldsymbol{C}]; \quad & J_2 = \mathrm{tr}[\boldsymbol{C}^2]; \quad J_3 = \mathrm{tr}[\boldsymbol{C}^3]; \quad J_4 = \mathrm{tr}[\boldsymbol{C}(\boldsymbol{M} \otimes \boldsymbol{M})]; \quad J_5 = \mathrm{tr}[\boldsymbol{C}^2(\boldsymbol{M} \otimes \boldsymbol{M})]; \\
& J_6 = \mathrm{tr}[\boldsymbol{D}_0 \otimes \boldsymbol{D}_0]; \quad J_7 = \mathrm{tr}[\boldsymbol{C}(\boldsymbol{D}_0 \otimes \boldsymbol{D}_0)]; \quad J_8 = \mathrm{tr}[\boldsymbol{C}^2(\boldsymbol{D}_0 \otimes \boldsymbol{D}_0)],
\end{aligned}
\tag{4.7}
$$

and $K_1^{\mathcal{D}_{\infty h}}, K_2^{\mathcal{D}_{\infty h}}$ are

$$K_1^{\mathcal{D}_{\infty h}} = \mathrm{tr}[(\boldsymbol{D}_0 \otimes \boldsymbol{D}_0)(\boldsymbol{M} \otimes \boldsymbol{M})]; \quad K_2^{\mathcal{D}_{\infty h}} = \mathrm{tr}[(\boldsymbol{D}_0 \otimes \boldsymbol{D}_0)\boldsymbol{C}(\boldsymbol{M} \otimes \boldsymbol{M})], \tag{4.8}$$

note that $J_1 \ldots J_5$ denote the mechanical invariants, $J_6 \ldots J_8$ denote the invariants introducing (isotropic) electro-mechanical effects and $K_1^{\mathcal{D}_{\infty h}}$ and $K_2^{\mathcal{D}_{\infty h}}$ are the two invariants responsible for introducing fibre dependent electro-mechanical effects.

Similarly, in the case of $\bar{e}_{\mathcal{C}_{\infty}}$, it yields

$$\bar{e}_{\mathcal{C}_{\infty}}(\boldsymbol{C}, \boldsymbol{D}_0, \boldsymbol{M}) = \hat{e}_{\mathcal{C}_{\infty}}(J_1, J_2, J_3, J_4, J_5, J_6, J_7, J_8, K_1^{\mathcal{C}_{\infty}}, K_2^{\mathcal{C}_{\infty}}), \tag{4.9}$$

---

[10] In the original Table 12 in [72], the invariant $\mathrm{tr}[\boldsymbol{C}^2(\boldsymbol{D}_0 \otimes \boldsymbol{D}_0)]$ is missing whilst the invariant $\mathrm{tr}[\boldsymbol{C}^2(\boldsymbol{D}_0 \otimes \boldsymbol{M})]$ is included in the basis. Notice that it is possible to show (refer to [54] and references therein) that either invariant can be expressed in terms of the rest of the invariants of the basis.

where the alternative fibre dependent electro-mechanical invariants are

$$K_1^{\mathcal{C}\infty} = \text{tr}[\boldsymbol{D}_0 \otimes \boldsymbol{M}]; \quad K_2^{\mathcal{C}\infty} = \text{tr}[\boldsymbol{C}(\boldsymbol{D}_0 \otimes \boldsymbol{M})]. \tag{4.10}$$

A further restriction, albeit not strictly necessary, is that of zero energy at the origin (i.e. $\mathcal{U}_0 = (\boldsymbol{F} = \boldsymbol{I}, \boldsymbol{D}_0 = \boldsymbol{0})$), that is, $e(\mathcal{U}_0) = 0$. However, an important restriction is that of zero stresses and electric field at the origin, namely,

$$\boldsymbol{P}(\mathcal{U}_0) = \partial_F e|_{\mathcal{U}_0} = \boldsymbol{0}; \qquad \boldsymbol{E}_0(\mathcal{U}_0) = \partial_{D_0} e\big|_{\mathcal{U}_0} = \boldsymbol{0}. \tag{4.11}$$

It is interesting to observe that for EAPs exhibiting symmetry of the group $\mathcal{D}_{\infty h}$, the electric field $\boldsymbol{E}_0$ evaluated at the origin of electric displacements, that is, $\boldsymbol{D}_0 = \boldsymbol{0}$ (regardless of the value of deformation), is zero, which is indeed the case as these materials do not experience any piezoelectric effects. This is obtained implicitly due to the dependence of the integrity basis on the second order tensor $\boldsymbol{D}_0 \otimes \boldsymbol{D}_0$ (refer to invariants $J_6 \ldots J_{10}$), that is,

$$\boldsymbol{E}_0(\boldsymbol{F}, \boldsymbol{D}_0 = \boldsymbol{0}) = \sum_{i=6}^{10} [(\partial_{I_i} \bar{e}_{\mathcal{D}\infty h})(\partial_{D_0 \otimes D_0} I_i)]\big|_{(\boldsymbol{F}, \boldsymbol{0})} 2 \underbrace{\boldsymbol{D}_0}_{=0} = \boldsymbol{0}. \tag{4.12}$$

However, for electro-active materials of the group $\mathcal{C}_\infty$, this restriction does not apply. Indeed, invariants $K_1^{\mathcal{C}\infty}$, $K_2^{\mathcal{C}\infty}$ depend linearly on $\boldsymbol{D}_0$ and not on $\boldsymbol{D}_0 \otimes \boldsymbol{D}_0$, which permits lifting of the restriction (4.12).

Finally, material characterisation typically requires calibration of material parameters at $\mathcal{U}_0$, that is

$$\mathcal{C}_e(\mathcal{U}_0) = \partial_{FF}^2 e|_{\mathcal{U}_0} = \mathcal{C}_e^{\text{lin}}; \quad \mathcal{Q}(\mathcal{U}_0) = \partial_{D_0 F}^2 e\big|_{\mathcal{U}_0} = \mathcal{Q}^{\text{lin}}; \quad \boldsymbol{\theta}(\mathcal{U}_0) = \partial_{D_0 D_0}^2 e\big|_{\mathcal{U}_0} = \boldsymbol{\theta}^{\text{lin}}, \tag{4.13}$$

or in case of using the Hessian components of the Helmholtz's free energy function $[\mathbb{H}_\Psi]$

$$\mathcal{C}_\Psi(\mathcal{W}_0) = \partial_{FF}^2 \Psi\big|_{\mathcal{W}_0} = \mathcal{C}_\Psi^{\text{lin}}; \quad \mathcal{P}(\mathcal{W}_0) = \partial_{D_0 F}^2 \Psi\big|_{\mathcal{W}_0} = \mathcal{P}^{\text{lin}}; \quad \boldsymbol{\epsilon}(\mathcal{W}_0) = \partial_{E_0 E_0}^2 \Psi\big|_{\mathcal{W}_0} = \boldsymbol{\epsilon}^{\text{lin}}, \tag{4.14}$$

where $\mathcal{W}_0 = (\boldsymbol{F} = \boldsymbol{I}, \boldsymbol{E}_0 = \boldsymbol{0})$.

4.2. $\mathcal{A}$-polyconvex transversely isotropic invariant representations

It is possible to re-express the above integrity bases of invariants $J_i, \{i = 1 \ldots 8\}$, $K_j^{\mathcal{D}\infty h}$, $K_j^{\mathcal{C}\infty}$, $\{j = 1, 2\}$ in terms of an alternative basis of invariants more amenable to the study of $\mathcal{A}$-polyconvexity. The purely mechanical isotropic invariants can be re-defined as

$$I_1 = J_1 = \boldsymbol{F} : \boldsymbol{F}; \qquad I_2 = \boldsymbol{H} : \boldsymbol{H}; \qquad I_3 = J, \tag{4.15}$$

where

$$J_2 = I_1^2 - 2I_2; \qquad J_3 = I_1^3 - 3I_1 I_2 + 3I_3^2. \tag{4.16}$$

The transversely isotropic mechanical invariants can be re-defined as

$$I_4 = J_4 = (\boldsymbol{F}\boldsymbol{M}) \cdot (\boldsymbol{F}\boldsymbol{M}); \qquad I_5 = (\boldsymbol{H}\boldsymbol{M}) \cdot (\boldsymbol{H}\boldsymbol{M}); \tag{4.17}$$

where

$$J_5 = I_1 I_4 - I_2 + I_5. \tag{4.18}$$

Similarly, the isotropic electro-mechanical invariants can be re-defined as

$$I_6 = J_6 = \boldsymbol{D}_0 \cdot \boldsymbol{D}_0; \qquad I_7 = J_7 = \boldsymbol{d} \cdot \boldsymbol{d}; \qquad I_8 = (\boldsymbol{H}\boldsymbol{D}_0) \cdot (\boldsymbol{H}\boldsymbol{D}_0), \tag{4.19}$$

where

$$J_8 = I_1 I_4 - I_2 + I_8, \tag{4.20}$$

and the transversely isotropic electro-mechanical contributions as

$$K_1^{\mathcal{D}\infty h} = (\boldsymbol{D}_0 \cdot \boldsymbol{M})^2; \qquad K_2^{\mathcal{D}\infty h} = (\boldsymbol{d} \cdot \boldsymbol{F}\boldsymbol{M})^2, \tag{4.21}$$

and

$$K_1^{\mathcal{C}_\infty} = \boldsymbol{D}_0 \cdot \boldsymbol{M}; \qquad K_2^{\mathcal{C}_\infty} = \boldsymbol{d} \cdot \boldsymbol{F}\boldsymbol{M}. \tag{4.22}$$

Thus, energies $\bar{e}_{\mathcal{D}_{\infty h}}$ and $\bar{e}_{\mathcal{C}_\infty}$ can be re-written as

$$\bar{e}_{\mathcal{D}_{\infty h}}(\boldsymbol{C}, \boldsymbol{D}_0, \boldsymbol{M}) = \hat{\bar{e}}_{\mathcal{D}_{\infty h}}(I_1, I_2, I_3, I_4, I_5, I_6, I_7, I_8, K_1^{\mathcal{D}_{\infty h}}, K_2^{\mathcal{D}_{\infty h}}); \tag{4.23a}$$

$$\bar{e}_{\mathcal{C}_\infty}(\boldsymbol{C}, \boldsymbol{D}_0, \boldsymbol{M}) = \hat{\bar{e}}_{\mathcal{C}_\infty}(I_1, I_2, I_3, I_4, I_5, I_6, I_7, I_8, K_1^{\mathcal{C}_\infty}, K_2^{\mathcal{C}_\infty}). \tag{4.23b}$$

It is customary to split the energy density into mechanical and electro-mechanical components, further splitting the former into isochoric and volumetric components, via suitable modification of the invariants I_1 and I_2. This can be formulated as follows

$$\begin{aligned} \bar{e}_{\mathcal{D}_{\infty h}}(\boldsymbol{C}, \boldsymbol{D}_0, \boldsymbol{m}) &= \tilde{e}_{\mathcal{D}_{\infty h}}^{\mathrm{iso,mec}}(I_1^{\mathrm{iso}}, I_2^{\mathrm{iso}}, I_4, I_5) + e^{\mathrm{vol}}(I_3) \\ &\quad + \tilde{e}_{\mathcal{D}_{\infty h}}^{\mathrm{ele}}(I_1, I_2, I_3, I_4, I_5, I_6, I_7, I_8, K_1^{\mathcal{D}_{\infty h}}, K_2^{\mathcal{D}_{\infty h}}); \end{aligned} \tag{4.24a}$$

$$\begin{aligned} \bar{e}_{\mathcal{C}_\infty}(\boldsymbol{C}, \boldsymbol{D}_0, \boldsymbol{m}) &= \tilde{e}_{\mathcal{C}_\infty}^{\mathrm{iso,mec}}(I_1^{\mathrm{iso}}, I_2^{\mathrm{iso}}, I_4, I_5) + e^{\mathrm{vol}}(I_3) \\ &\quad + \tilde{e}_{\mathcal{C}_\infty}^{\mathrm{ele}}(I_1, I_2, I_3, I_4, I_5, I_6, I_7, I_8, K_1^{\mathcal{C}_\infty}, K_2^{\mathcal{C}_\infty}), \end{aligned} \tag{4.24b}$$

where the different energetic contributions are identified by corresponding upper indices and where

$$I_1^{\mathrm{iso}} = I_3^{-2/3} I_1 = J^{-2/3} \boldsymbol{F} : \boldsymbol{F}; \qquad I_2^{\mathrm{iso}} = I_3^{-4/3} I_2 = J^{-4/3} \boldsymbol{H} : \boldsymbol{H}. \tag{4.25}$$

It is now possible to construct polyconvex energy density functions by combining (1) a convex (with respect to invariant I_3) volumetric energy e^{vol} contribution and (2) a polyconvex isochoric energy density contribution. To accomplish the latter, it is possible to use a linear combination (with positive weighting coefficients) of $\mathcal{A}$-polyconvex invariants I_1, I_2, I_1^{iso}, I_4, I_5, I_6, I_7, $K_1^{\mathcal{D}_{\infty h}}$, and $K_1^{\mathcal{C}_\infty}$. Notice that as invariants I_2^{iso}, I_8, $K_2^{\mathcal{D}_{\infty h}}$, and $K_2^{\mathcal{C}_\infty}$ are not rank-one convex, thus, they are not $\mathcal{A}$-polyconvex and cannot be arbitrarily used for the construction of the isochoric energy density. A potential way around this issue can be through the careful selection of the weighting coefficients so that the $\mathcal{A}$-polyconvex invariants compensate those non $\mathcal{A}$-polyconvex.

Yet another more robust possibility (preferred in this paper) consists of *polyconvexifying* the non $\mathcal{A}$-polyconvex invariants, cf [57,62,70] so that a straight linear combination of invariants can then be used. Polyconvexification is, in general, not trivial and may potentially lead to the onset of non-coercive terms. Such modification has to be designed case by case, e.g., I_2^{iso} can be modified to

$$I_{2,\mathrm{pol}}^{\mathrm{iso}} = \left(I_2^{\mathrm{iso}}\right)^{3/2} = J^{-2}\left(\boldsymbol{H} : \boldsymbol{H}\right)^{3/2}, \tag{4.26}$$

which is polyconvex [70]. Similarly, a possible polyconvex invariant expression for I_8 is

$$I_{8,\mathrm{pol}} = \alpha^2 \left(\boldsymbol{H} : \boldsymbol{H}\right)^2 + \beta^2 \left(\boldsymbol{D}_0 \cdot \boldsymbol{D}_0\right)^2 + \alpha\beta(\boldsymbol{H}\boldsymbol{D}_0) \cdot (\boldsymbol{H}\boldsymbol{D}_0) = \alpha^2(I_2)^2 + \beta^2(I_6)^2 + \alpha\beta(I_8), \tag{4.27}$$

where α, β are positive material constants. Analogously, a possible modification of $K_2^{\mathcal{C}_\infty}$ is

$$K_{2,\mathrm{pol}}^{\mathcal{C}_\infty} = (\eta\boldsymbol{d} + \psi\boldsymbol{F}\boldsymbol{M}) \cdot (\eta\boldsymbol{d} + \psi\boldsymbol{F}\boldsymbol{M}) = \eta^2 I_7 + \psi^2 I_4 + 2\eta\psi K_2^{\mathcal{C}_\infty}, \tag{4.28}$$

where η, ψ are positive material constants. Finally, $K_2^{\mathcal{D}_{\infty h}}$ can be replaced with

$$K_{2,\mathrm{pol}}^{\mathcal{D}_{\infty h}} = \left((\alpha_1\boldsymbol{D}_0 + \alpha_2\boldsymbol{M}) \cdot (\alpha_1\boldsymbol{D}_0 + \alpha_2\boldsymbol{M}) + (\alpha_3\boldsymbol{d} + \alpha_4\boldsymbol{F}\boldsymbol{M}) \cdot (\alpha_3\boldsymbol{d} + \alpha_4\boldsymbol{F}\boldsymbol{M})\right)^2, \tag{4.29}$$

where α_i, $i = 1 \dots 4$ are positive material constants. Notice that above invariant $K_{2,\mathrm{pol}}^{\mathcal{D}_{\infty h}}$ in (4.29) contains the term $8\alpha_1\alpha_2\alpha_3\alpha_4 K_2^{\mathcal{D}_\infty}$. Unfortunately, such convexification also contains the term $4\alpha_1\alpha_2\alpha_4^2 K_1^{\mathcal{C}_\infty} I_4$, which is piezoelectric (linear with respect to $\boldsymbol{D}_0$) and cannot be generated from the integrity basis of the anisotropy group $\mathcal{D}_\infty$. Instead, this invariant is valid for the anisotropy group $\mathcal{C}_\infty$, as it is formed as product of invariants $K_1^{\mathcal{C}_\infty}$ and I_4, both in the integrity basis of the referred group. In order to remedy this shortcoming, we propose to replace invariant $K_2^{\mathcal{D}_\infty}$ with an alternative invariant $\widetilde{K}_2^{\mathcal{D}_\infty}$ defined as

$$\widetilde{K}_2^{\mathcal{D}_\infty} = \left(K_2^{\mathcal{C}_\infty}\right)^2 = (\boldsymbol{d} \cdot \boldsymbol{F}\boldsymbol{M})^2, \tag{4.30}$$

followed by the introduction of the following polyconvex counterpart $\widetilde{K}_{2,\mathrm{pol}}^{\mathcal{D}_\infty}$ defined as

$$\widetilde{K}_{2,\mathrm{pol}}^{\mathcal{D}_\infty} = I_7^2 + \widetilde{K}_2^{\mathcal{D}_\infty} + I_4^2. \tag{4.31}$$

Clearly, above polyconvex invariant $\widetilde{K}_{2,\mathrm{pol}}^{\mathcal{D}_\infty}$ is comprised of invariants which are part of the integrity basis of the anisotropy group $\mathcal{D}_\infty$.

Proof of polyconvexity of invariants $I_{8,\mathrm{pol}}$, $\widetilde{K}_2^{\mathcal{D}_{\infty h}}$ and $K_{2,\mathrm{pol}}^{\mathcal{C}_\infty}$ is included in Appendix A.2. Additionally, in order to fulfil assumptions of Theorem 3.1, we need to ensure that the energy is coercive, cf. (3.23). For example, invariant $K_1^{\mathcal{C}_\infty} = \boldsymbol{D}_0 \cdot \boldsymbol{M}$ is $\mathcal{A}$-polyconvex, but not coercive. Notice that $\boldsymbol{D}_0 \cdot \boldsymbol{M} = 0$ if $\boldsymbol{D}_0$ is perpendicular to $\boldsymbol{M}$. To ensure coercivity of the overall energy e, we must combine non-coercive invariants with coercive ones, e.g., $aI_6 + bK_1^{\mathcal{C}_\infty}$ is coercive for $a > 0$.

5. Numerical examples

This section presents a series of numerical examples modelling the performance of transversely isotropic EAPs at large strains. The first numerical example, restricted to the case of homogeneous deformation, circumvents the need to use a Finite Element (FE) spatial discretisation and studies the behaviour, at a local level, of the response of the EAP. A comprehensive study will be conducted where the influence of the deformation and the level of transverse anisotropy has on the stability of the model. In addition, polyconvex and non-polyconvex constitutive models will be studied and compared for a range of deformations and electric fields, emphasising that seemingly similar models might lead to unexpected results. The rest of numerical examples abandon the assumption of uniform deformation. The second example explores the use of three-dimensional Finite Elements in the case of transversely isotropic EAPs in the form of thin rectangular films subjected to appropriate mechanical and electrical boundary conditions. The influence of the orientation of the vector of anisotropy and electro-mechanical properties will be studied, especially into their effect on the stability of the model, so as to prevent the onset of spurious mesh dependence results. The third example explores the effect of anisotropy orientation on the development of wrinkling patterns in a thin EAP film. The final example explores the twisting behaviour of a piezoelectric-type material.

5.1. Numerical example 1

Through this example we aim to:

- Analyse the response of $\mathcal{A}$-polyconvex and non-$\mathcal{A}$-polyconvex energy functionals in homogeneous states of deformation and electric field.
- Appreciate the importance of using arc-length techniques in order to bypass instability regions and harness actuator performance beyond the moderate regime.

We consider a prototypical set-up very similar to that already explored by several authors in the past, both numerically [87,88] and experimentally [89]. This consists of a Dielectric Elastomer film, such as the one depicted in Fig. 2, which is subjected to a homogeneous state of deformation and electric field. Two electrodes are placed at opposite faces of the film and an externally controlled Lagrangian electric field $\boldsymbol{E}_0$ is applied across and orientated along the X_3 axis, whilst maintaining stress-free conditions, in turn generating a state of uniform deformation and electric displacement across the film. This uniform state of deformation and electric field is exploited in order to study the response of the elastomer from a local point of view, without the need to resort to a finite element discretisation. As a result, in the absence of any further loads and electric charges, the homogeneous solution to this problem corresponds to the stationary points $\{\boldsymbol{F}^*, \boldsymbol{D}_0^*\}$ of the Helmholtz's free energy functional defined as

$$\Pi(\boldsymbol{F}^*, \boldsymbol{D}_0^*, \boldsymbol{E}_0) = \inf_{\boldsymbol{F}} \inf_{\boldsymbol{D}_0} \{e(\boldsymbol{F}, \boldsymbol{D}_0) - \boldsymbol{E}_0 \cdot \boldsymbol{D}_0\}, \tag{5.1}$$

where $\boldsymbol{E}_0$ is the externally controlled electric field. Thus, the stationary conditions of the above functional arise as

$$\mathcal{R}_{\boldsymbol{F}}(\boldsymbol{F}, \boldsymbol{D}_0) = \partial_{\boldsymbol{F}} e = \boldsymbol{0}; \qquad \mathcal{R}_{\boldsymbol{D}_0}(\boldsymbol{F}, \boldsymbol{D}_0) = \partial_{\boldsymbol{D}_0} e - \boldsymbol{E}_0 = \boldsymbol{0}. \tag{5.2}$$

The above nonlinear stationary conditions (5.2) are solved in terms of unknowns $\boldsymbol{F}^*$ and $\boldsymbol{D}_0^*$ dependent upon the externally controlled electric field $\boldsymbol{E}_0$. A similar set-up has been previously used in many Refs. [31,36], albeit restricted to the condition of plane strain and strict incompressibility. Here, these kinematic assumptions
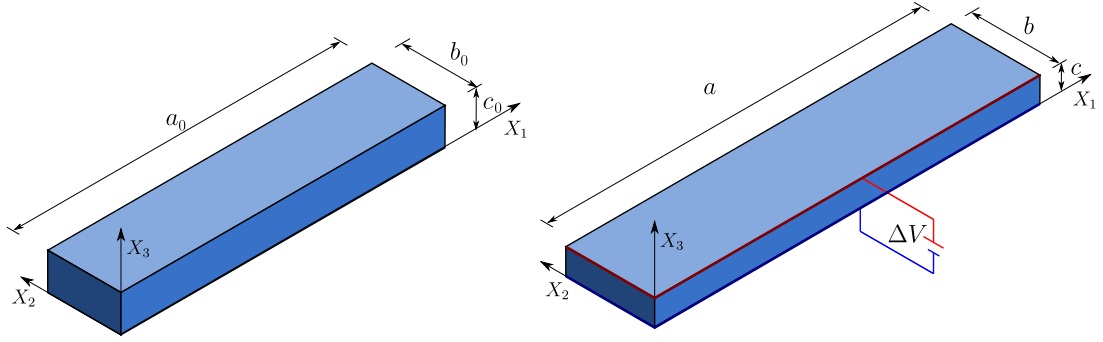
Fig. 2. Numerical example 1. Experimental set-up. The application of a uniform electric field along the OX_3 direction causes a stretch of the DE laminated composite along OX_1 direction.

are relaxed and the deformation gradient tensor is left to adopt a more complex expression. Specifically, $\boldsymbol{F}$ and $\boldsymbol{E}_0$ are formulated as

$$\boldsymbol{F} = \begin{bmatrix} F_{11} & 0 & 0 \\ 0 & F_{22} & 0 \\ 0 & 0 & F_{33} \end{bmatrix}; \qquad \boldsymbol{E}_0 = \begin{bmatrix} 0 \\ 0 \\ E_0 \end{bmatrix}, \tag{5.3}$$

Typically, F_{33} is constrained through the condition of strict incompressibility, as this permits to obtain closed-form solutions to the problem. Notice that these simplifying assumption does not apply to this study, where the nonlinear stationary conditions (5.2) are solved by an iterative Newton–Raphson method. In addition, in order to track the entire equilibrium path beyond the onset of limit points (i.e., snap-through, snap-back), an arc-length technique is employed. Two constitutive models have been considered in this study. The first restricts to the isotropic case whereas the second considers the case of the transversely isotropic symmetry group $\mathcal{D}_\infty$.

5.1.1. Isotropic case

For the isotropic case, two energy functionals have been considered. The first, denoted as $\bar{e}_{iso,1}(\boldsymbol{F}, \boldsymbol{D}_0)$ is given in Eq. (5.4) and it has been additively decomposed into two terms. The first represents strain energy of a Mooney–Rivlin model and that of an ideal dielectric elastomer. This entire contribution has been denoted as $\bar{e}_{ID}(\boldsymbol{F}, \boldsymbol{D}_0)$. The second term in the additive decomposition contains the non-$\mathcal{A}$-polyconvex invariant $I_8(\boldsymbol{F}, \boldsymbol{D}_0)$.

$$\bar{e}_{iso,1}(\boldsymbol{F}, \boldsymbol{D}_0) = \bar{e}_{ID}(\boldsymbol{F}, \boldsymbol{D}_0) + \frac{1}{\varepsilon_2} I_8(\boldsymbol{F}, \boldsymbol{D}_0);$$

$$\bar{e}_{ID}(\boldsymbol{F}, \boldsymbol{D}_0) = \frac{\mu_1}{2} I_1^{iso}(\boldsymbol{F}) + \frac{\mu_2}{2} I_2^{iso}(\boldsymbol{F}) + \frac{\lambda}{2}(I_3(\boldsymbol{F}) - 1)^2 + \frac{1}{2\varepsilon_1} \frac{I_7(\boldsymbol{F}, \boldsymbol{D}_0)}{I_3(\boldsymbol{F})} \tag{5.4}$$

where

$$I_8(\boldsymbol{F}, \boldsymbol{D}_0) = \boldsymbol{H}\boldsymbol{D}_0 \cdot \boldsymbol{H}\boldsymbol{D}_0. \tag{5.5}$$

Furthermore, a second energy functional, denoted as $\bar{e}_{iso,1}(\boldsymbol{F}, \boldsymbol{D}_0)$ has been considered. This is also additively decomposed into the $\bar{e}_{ID}(\boldsymbol{F}, \boldsymbol{D}_0)$ and the additional invariant $I_{8,pol}$, which results from the polyconvexification of I_8. The explicit expression for $\bar{e}_{iso,1_{pol}}(\boldsymbol{F}, \boldsymbol{D}_0)$ can be seen in Eq. (5.6), i.e.

$$\bar{e}_{iso,1_{pol}}(\boldsymbol{F}, \boldsymbol{D}_0) = \bar{e}_{ID}(\boldsymbol{F}, \boldsymbol{D}_0) + I_{8,pol}(\boldsymbol{F}, \boldsymbol{D}_0) - 12\alpha^2 \log(I_3(\boldsymbol{F})), \tag{5.6}$$

where

$$I_{8,pol} = \alpha^2 I_2(\boldsymbol{F}) + \alpha\beta I_8 + \beta^2 I_6^2(\boldsymbol{D}_0). \tag{5.7}$$

For the non-$\mathcal{A}$-polyconvex model in (5.4), the values of the material parameters can be found in Table 1. For the $\mathcal{A}$-polyconvex model in (5.6), five combinations of material parameters can be found in Table 2. It can be seen that the material parameters $\{\mu_1\mu_2, \lambda, \varepsilon\}$ for the polyconvex models have been kept the same as their counterparts $\{\mu_1\mu_2, \lambda, \varepsilon_1\}$, respectively, for the non-polyconvex case. Several values for the two remaining material parameters

Table 1

Material properties for constitutive model in Eq. (5.4).

μ_1	μ_2	λ	ε_1	ε_2
1×10^5	$1.0\mu_1$	$10^3\mu_1$	$4.82\varepsilon_0$	$24\varepsilon_0$

Table 2

Material properties for the constitutive model in Eq. (5.6).

Parameters	Pol. Mat. 1	Pol. Mat. 2	Pol. Mat. 3	Pol. Mat. 4	Pol. Mat. 5
μ_1	10^5	10^5	10^5	10^5	10^5
μ_2	10^5	10^5	10^5	10^5	10^5
λ	10^8	10^8	10^8	10^8	10^8
ε	$4.82\varepsilon_0$	$4.82\varepsilon_0$	$4.82\varepsilon_0$	$4.82\varepsilon_0$	$4.82\varepsilon_0$
α	1.78×10^8	2.90×10^9	4.91×10^9	6.92×10^9	8.93×10^9
β	2.52×10^2	4.11×10^3	6.95×10^3	9.80×10^3	1.26×10^4

$\{\alpha, \beta\}$ have been considered in order to see their influence in the equilibrium path of the elastomer. From Fig. $3_{a,b}$, the combination of values for $\{\alpha, \beta\}$ that yields a closer response to the non-polyconvex model is that corresponding with the polyconvex material 2 (Pol. Mat. 2), whose values for $\{\alpha, \beta\}$ can be found in the third column of Table 2. These values have been determined by performing an optimisation problem. Specifically, for each pair of values $(\boldsymbol{F}, \boldsymbol{D}_0)$ in the equilibrium path of the non-polyconvex model, we have formulated the following minimisation problem

$$\min_{\alpha,\beta} \begin{cases} \mathcal{J} \\ \text{s.t. } \alpha > 0, \ \beta > 0 \end{cases} \tag{5.8}$$

where the objective function $\mathcal{J}$ is defined as

$$\mathcal{J} = \sqrt{\sum_{i=1}^{n} ||\partial_{\boldsymbol{F}}\bar{e}_{\text{iso},1_{\text{pol}}}(\boldsymbol{F}_i, \boldsymbol{D}_{0i})||^2} + \sqrt{\sum_{i=1}^{n} \frac{||\partial_{\boldsymbol{D}_0}\bar{e}_{\text{iso},1_{\text{pol}}}(\boldsymbol{F}_i, \boldsymbol{D}_{0i}) - \partial_{\boldsymbol{D}_0}\bar{e}_{\text{iso},1}(\boldsymbol{F}_i, \boldsymbol{D}_{0i})||^2}{||\partial_{\boldsymbol{D}_0}\bar{e}_{\text{iso},1}(\boldsymbol{F}_i, \boldsymbol{D}_{0i})||^2}}, \tag{5.9}$$

where n refers to the number of discrete data pairs $(\boldsymbol{F}, \boldsymbol{D}_0)$ describing the discrete equilibrium path of the non-polyconvex model.

The similarity between the equilibrium paths of the non-polyconvex model and that whose material parameters $\{\alpha, \beta\}$ have been obtained through the optimisation method described above is very reasonable up to a 10% in the F_{11} component of the deformation gradient tensor, beyond which both equilibrium paths start diverging (see Fig. 3). Clearly, this is due to the fact that the polyconvex model contains higher nonlinear terms I_4^2 and I_6^2, yielding a slightly more stable response to that of its non-polyconvex counterpart. From Fig. 3, it is possible to observe the regions where the Hessian operator loses positive definiteness and hence, where the loss of convexity occurs. Interestingly, the non-polyconvex model loses also ellipticity (see the yellow region in Fig. 3_c). This has been checked by monitoring the least of the minors of the acoustic tensor $\boldsymbol{Q}$ in Eq. (3.14). Evidently, this is not appreciated in any of the five $\mathcal{A}$-polyconvex models in Fig. 3_{d-h}.

5.1.2. Anisotropic case

In this example, we consider the transversely anisotropic group $\mathcal{D}_{\infty h}$. Two energy density functions are considered. The first, denoted as $\bar{e}_{\mathcal{D}_{\infty h},1}(\boldsymbol{F}, \boldsymbol{D}_0, \boldsymbol{M})$, is not $\mathcal{A}$-polyconvex. This is additively decomposed into the isotropic density function $\bar{e}_{\text{ID}}(\boldsymbol{F}, \boldsymbol{D}_0)$ ($\mathcal{A}$-polyconvex) and the non-polyconvex invariant $K_2^{\mathcal{D}_{\infty h},1}(\boldsymbol{F}, \boldsymbol{D}_0, \boldsymbol{M})$

$$\bar{e}_{\mathcal{D}_{\infty h},1}(\boldsymbol{F}, \boldsymbol{D}_0, \boldsymbol{M}) = \bar{e}_{\text{ID}}(\boldsymbol{F}, \boldsymbol{D}_0) + \frac{1}{\varepsilon_2}K_2^{\mathcal{D}_{\infty h}}(\boldsymbol{F}, \boldsymbol{D}_0, \boldsymbol{M}), \tag{5.10}$$

where

$$K_2^{\mathcal{D}_{\infty h}}(\boldsymbol{F}, \boldsymbol{D}_0) = (\boldsymbol{d} \cdot \boldsymbol{F}\boldsymbol{M})^2. \tag{5.11}$$
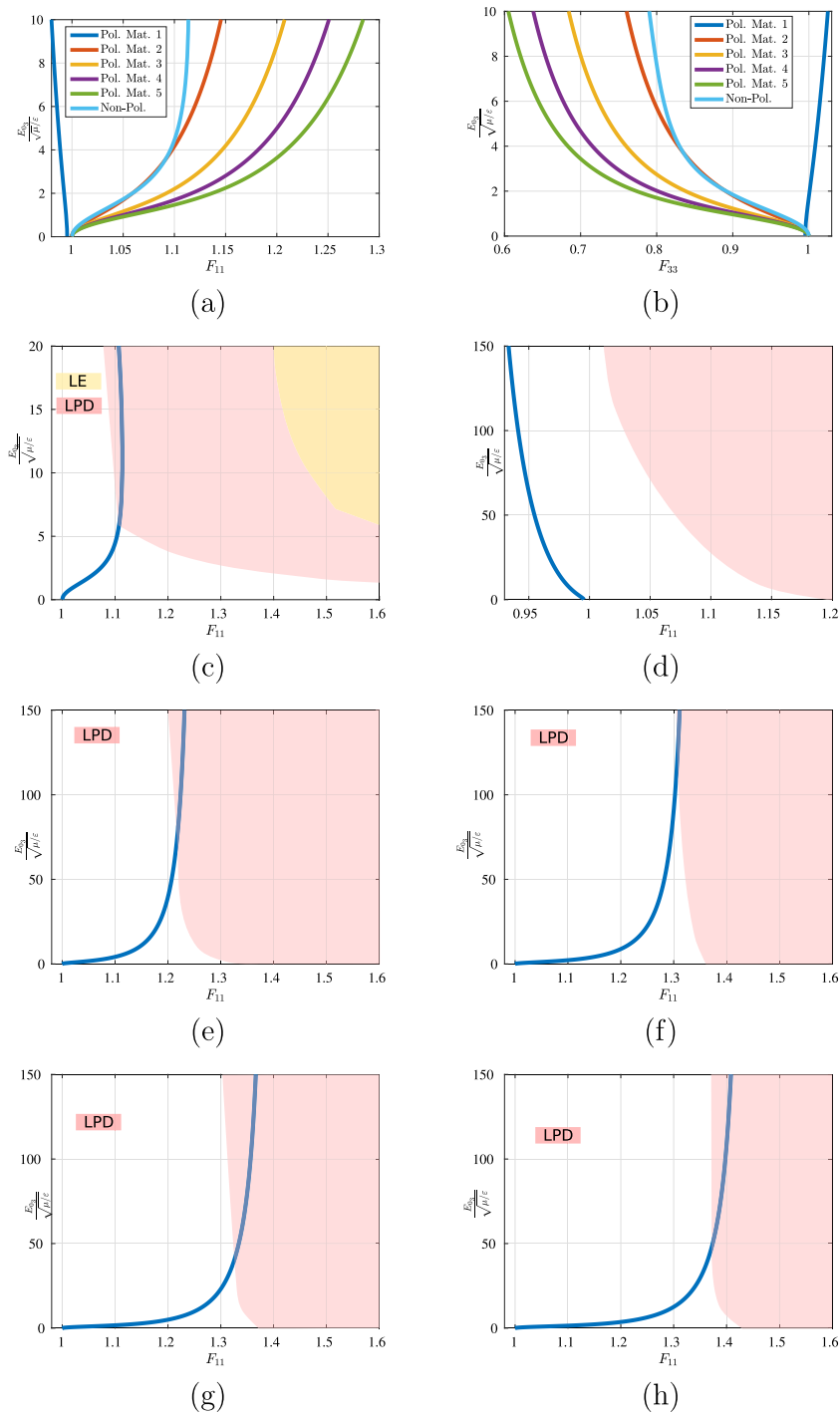
Fig. 3. (a)–(b) Equilibrium paths for non-polyconvex model in Eq. (5.4) with material properties in Table 1 and for the five polyconvex models (see Eq. (5.6)) with material parameters in Table 2. (c)–(h) represent the regions where loss of positive definiteness (LPD) of the Hessian operator and loss of ellipticity (LE) occurs for the non-polyconvex and polyconvex models. The reference values for the dimensionless electric field are $\mu = 10^5$ and $\varepsilon = 4.8\varepsilon_0$. (For interpretation of the references to colour in this figure legend, the reader is referred to the web version of this article.)

Table 3
Material properties for non-polyconvex model in Eq. (5.10).

μ_1	μ_2	λ	ε_1	ε_2
1×10^5	$1.0\mu_1$	$10^3\mu_1$	$4.82\varepsilon_0$	$24\varepsilon_0$

Table 4
Material parameters for polyconvex model in Eq. (5.12).

Parameters	Pol. Mat. 1	Pol. Mat. 2	Pol. Mat. 3	Pol. Mat. 4	Pol. Mat. 5
μ_1	3.67×10^5	6.30×10^5	5.12×10^5	0.44	8.33×10^5
μ_2	21.86	9.56×10^3	6.25×10^3	2.87×10^{-2}	0.25
λ	10^8	10^8	10^8	10^8	10^8
ε_1	$7.48\varepsilon_0$	$9.6\varepsilon_0$	12.36	$4.9\varepsilon_0$	$9.6\varepsilon_0$
α	3.97×10^6	4.20×10^6	6.50×10^6	1.27×10^7	2.47×10^6
β	110.13	0.232	37.40	193.12	1.42×10^{-2}

The material parameters $\{\mu_1, \mu_2, \lambda, \varepsilon_1, \varepsilon_2\}$ featuring in the resulting non-polyconvex model $\bar{e}_{\mathcal{D}_{\infty h,1}}(\boldsymbol{F}, \boldsymbol{D}_0, \boldsymbol{M})$ can be found in Table 3.

The second strain energy density function considered, denoted as $\bar{e}^{\text{pol}}_{\mathcal{D}_{\infty h,1}}(\boldsymbol{F}, \boldsymbol{D}_0, \boldsymbol{M})$ can be seen in Eq. (5.12). Notice that, in contrast to Eq. (5.10), the non-polyconvex invariant $K_2^{\mathcal{D}_{\infty h,1}}(\boldsymbol{F}, \boldsymbol{D}_0, \boldsymbol{M})$ has been replaced with its polyconvex counterpart $K_{2,\text{pol}}^{\mathcal{D}_{\infty h}}(\boldsymbol{F}, \boldsymbol{D}_0, \boldsymbol{M})$ and an additional term (third term on the right hand side of (5.12)) which guarantees the stress-free condition in the origin, namely

$$\bar{e}^{\text{pol}}_{\mathcal{D}_{\infty h,1}}(\boldsymbol{F}, \boldsymbol{D}_0, \boldsymbol{M}) = \bar{e}_{\text{ID}}(\boldsymbol{F}, \boldsymbol{H}, J, \boldsymbol{d}) + K_{2,\text{pol}}^{\mathcal{D}_{\infty h}}(\boldsymbol{F}, \boldsymbol{D}_0, \boldsymbol{M}) + \beta^2\Big(I_5(\boldsymbol{F}, \boldsymbol{M}) - \log(I_3(\boldsymbol{F}))\Big);$$

$$K_{2,\text{pol}}^{\mathcal{D}_{\infty h}}(\alpha_1, \alpha_2, \alpha_3, \alpha_4, \boldsymbol{F}, \boldsymbol{D}_0, \boldsymbol{M}) = \alpha^2 I_7^2(\boldsymbol{F}, \boldsymbol{D}_0) + \alpha\beta K_2^{\mathcal{D}_{\infty h}}(\boldsymbol{F}, \boldsymbol{D}_0) + \beta^2 I_4^2(\boldsymbol{F}, \boldsymbol{M}).$$

$$(5.12)$$

For all the models, the preferred direction $\boldsymbol{M}$ was set to $\boldsymbol{M} = \begin{bmatrix} 0 & 0 & 1 \end{bmatrix}^T$.

For the $\mathcal{A}$-polyconvex model in (5.12), five combinations of material parameters can be found in Table 4. Unlike in the isotropic case, (where $\{\mu_1, \mu_2, \lambda, \varepsilon_1\}$) kept the same values as the non-polyconvex model, in this case, all the six material parameters $\{\mu_1, \mu_2, \lambda, \varepsilon_1, \alpha, \beta\}$ have been varied in order to observed their influence in the equilibrium path of the resulting polyconvex model. This can be observed in Fig. 4$_{a,b}$. From this figure, the combination of values for $\{\mu_1, \mu_2, \lambda, \varepsilon_1, \alpha, \beta\}$ depends on the interval of $\boldsymbol{F}$ where the optimisation problem described in that yields a closer response to the non-polyconvex model is that corresponding with the polyconvex material 2 (Pol. Mat. 2), whose values for $\{\alpha, \beta\}$ can be found in the third column of Table 2. These values have been determined by performing an optimisation problem. Specifically, for each pair of values $(\boldsymbol{F}, \boldsymbol{D}_0)$ in the equilibrium path of the non-polyconvex model, we have formulated the following minimisation problem (5.8) was carried out. This entails that the minimisation problem in this case can be reformulated as

$$\min_{\mu_1, \mu_2, \lambda, \varepsilon_1, \alpha, \beta} \begin{cases} \mathcal{J} \\ \text{s.t. } \{\mu_1, \mu_2, \lambda, \epsilon_1, \alpha, \beta\} > 0 \end{cases} \tag{5.13}$$

where the objective function $\mathcal{J}$ is defined as

$$\mathcal{J} = \sqrt{\sum_{i=n_1}^{n_2} ||\partial_{\boldsymbol{F}} \bar{e}^{\text{pol}}_{\mathcal{D}_{\infty h,1}}(\boldsymbol{F}_i, \boldsymbol{D}_{0i})||^2} + \sqrt{\sum_{i=n_1}^{n_2} \frac{||\partial_{\boldsymbol{D}_0} \bar{e}^{\text{pol}}_{\mathcal{D}_{\infty h,1}}(\boldsymbol{F}_i, \boldsymbol{D}_{0i}) - \partial_{\boldsymbol{D}_0} \bar{e}_{\mathcal{D}_{\infty h,1}}(\boldsymbol{F}_i, \boldsymbol{D}_{0i})||^2}{||\partial_{\boldsymbol{D}_0} \bar{e}^{\text{pol}}_{\mathcal{D}_{\infty h,1}}(\boldsymbol{F}_i, \boldsymbol{D}_{0i})||^2}}, \tag{5.14}$$

where n_1 and n_2 refer to the initial and final elements within the set $\boldsymbol{F}_i, \boldsymbol{D}_{0i}$, describing the discrete equilibrium path of the non-polyconvex model, which are considered for the optimisation problem. It can be seen that case corresponding with the polyconvex material 4 (Pol. Mat. 4 in Fig. 4$_{a,b}$, with material parameters in the fifth column of Table 4) fits the non-polyconvex model extremely well for values of F_{11} close to 1. However, this agreement disappears beyond this point and both models are extremely dissimilar past this point. On the other hand, the case
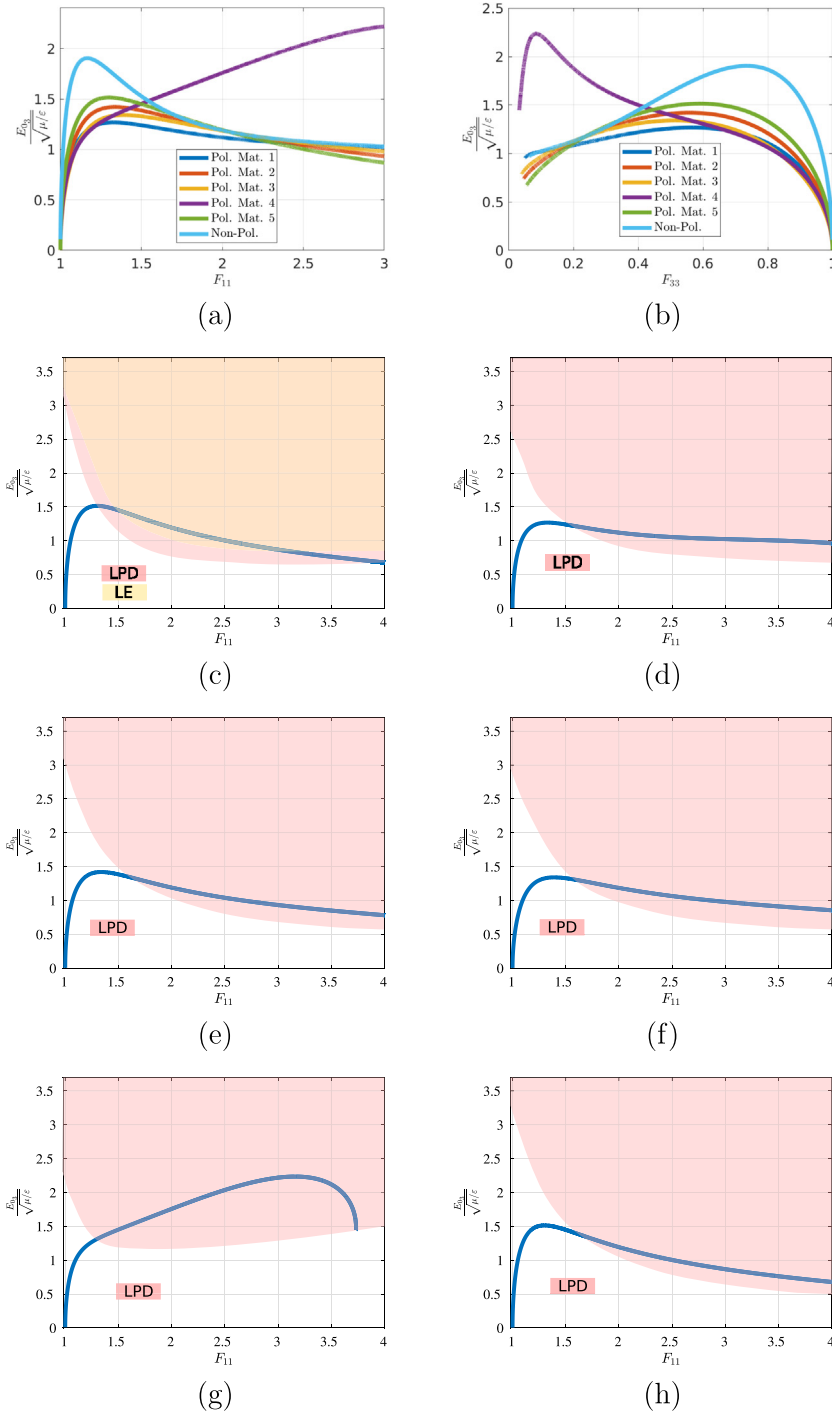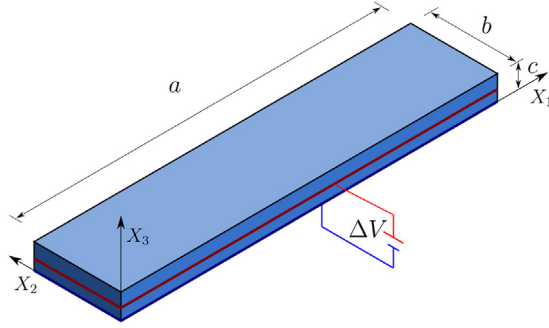
Fig. 4. (a)–(b) Equilibrium paths for non-polyconvex model in Eq. (5.10) with material properties in Table 3 and for the five polyconvex models (see Eq. (5.12)) with material parameters in Table 4. (c)–(h) represent the regions where loss of positive definiteness (LPD) of the Hessian operator and loss of ellipticity (LE) occurs for the non-polyconvex and polyconvex models. The reference values for the dimensionless electric field are $\mu = 10^5$ and $\varepsilon = 4.8\varepsilon_0$. (For interpretation of the references to colour in this figure legend, the reader is referred to the web version of this article.)

Fig. 5. Problem setting.

corresponding with the polyconvex material 1 (Pol. Mat. 1 in Fig. 4$_{a,b}$, with material parameters in the second column of Table 4), only fits very well the equilibrium path of the non-polyconvex model for high values of F_{11}.

From Fig. 4, it is possible to observe the regions where the Hessian operator loses positive definiteness and hence, where the loss of convexity occurs. Interestingly, the non-polyconvex model loses in addition ellipticity (see the yellow region in Fig. 4$_c$). This has been checked by monitoring the least of the minors of the acoustic tensor $\boldsymbol{Q}$ in Eq. (3.14). Evidently, this is not appreciated in any of the five $\mathcal{A}$-polyconvex models in Fig. 4$_{d-h}$.

5.2. Numerical example 2

The objective of this example are to:

- Demonstrate the influence of the fibre orientation on the mode of deformation of the EAP in the case of bending in a realistic three-dimensional setting.
- Study the loss of the generalised rank-one convexity.

Note that a similar example exploring the effect of fibre orientation on bending and twisting actuation of a fibre-reinforced magneto-elastomer has been studied in [90]. The ratio between length a, width b, and height c of the EAP are taken as $c = a/50$, $b = a/6$. The sample, depicted in Fig. 5, is clamped at one end and is loaded by the application of electric potential in the electrodes in the bottom and in the middle of the height. $\Delta V = \Lambda h \sqrt{\mu_1/\varepsilon_1}$ where Λ is a loading parameter, and μ_1 and ε_1 are material parameters, see Table 5. Note that the specimen was discretised with $120 \times 20 \times 6$ elements and the calculations are performed using the mixed Hu–Washizu variational principle, see Appendix A.3 for more details. In addition, two different material models are considered. $\mathcal{D}_{\infty h}$ symmetry applicable to electroactive polymers, is assumed in both cases.

5.2.1. Model 1: $\mathcal{A}$-polyconvex constitutive law

The energy is constructed to be $\mathcal{A}$-polyconvex meaning that it is composed of $\mathcal{A}$-polyconvex invariants only. The proposed model is defined through the energy written as

$$\bar{e}_{\mathcal{D}_{\infty h},1}(\boldsymbol{F}, \boldsymbol{D}_0, \boldsymbol{M}) = \bar{e}_1(\boldsymbol{F}) + \bar{e}_2(\boldsymbol{F}, \boldsymbol{M}) + \bar{e}_3(\boldsymbol{F}, \boldsymbol{D}_0) + \bar{e}_4(\boldsymbol{F}, \boldsymbol{D}_0, \boldsymbol{M}), \tag{5.15a}$$

$$\bar{e}_1(\boldsymbol{F}) = \frac{\mu_1}{2} I_1^{\text{iso}}(\boldsymbol{F}) + \frac{\mu_2}{2} I_{2,\text{pol}}^{\text{iso}}(\boldsymbol{F}) + \frac{\lambda}{2}(I_3(\boldsymbol{F}) - 1)^2, \tag{5.15b}$$

$$\bar{e}_2(\boldsymbol{F}, \boldsymbol{M}) = \frac{\mu_3}{2\alpha} I_4^\alpha(\boldsymbol{F}, \boldsymbol{M}) + \frac{\mu_3}{2\beta} I_5^\beta(\boldsymbol{F}, \boldsymbol{M}) - \mu_3 \ln I_3(\boldsymbol{F}), \tag{5.15c}$$

$$\bar{e}_3(\boldsymbol{F}, \boldsymbol{D}_0) = \frac{1}{2\varepsilon_1} \frac{I_7(\boldsymbol{F}, \boldsymbol{D}_0)}{I_3(\boldsymbol{F})} + \frac{1}{2\varepsilon_2} I_6(\boldsymbol{D}_0), \tag{5.15d}$$

$$\bar{e}_4(\boldsymbol{D}_0) = \frac{1}{2\varepsilon_3} K_1^{\mathcal{D}_{\infty h}}(\boldsymbol{D}_0). \tag{5.15e}$$

Naturally, to assure $\mathcal{A}$-polyconvexity of the model, positive material constants have to be chosen, which is a reasonable physical requirement leading also to coercivity. The material constants used in the following simulation are presented in Table 5.

Table 5
Material properties for Material model 1.

μ_1	μ_2	μ_3	λ	ε_1	ε_2	ε_3	α	β
1×10^5	$1.0\mu_1$	$1.0\mu_1$	$10^3 \times \mu_1$	$9.6\varepsilon_0$	$2.88\varepsilon_0$	$1.92\varepsilon_0$	1	1

We study three samples with fibre alignment of $0°$, $45°$, and $90°$ and evaluate the influence of the fibre orientation upon the electrical loading. The three aforementioned fibre orientations correspond to $\boldsymbol{M}_0 = \begin{bmatrix} 1 & 0 & 0 \end{bmatrix}^T$, $\boldsymbol{M}_{45} = \begin{bmatrix} 1/\sqrt{2} & 1/\sqrt{2} & 0 \end{bmatrix}^T$, and $\boldsymbol{M}_{90} = \begin{bmatrix} 0 & 1 & 0 \end{bmatrix}^T$ respectively. The results of simulation are depicted in Fig. 6 showing clearly that design of fibres alignment substantially influence response of an EAP leading to bending, twisting, or combined modes of deformation. Therefore, the computational approach can be used to carefully tailor the fibre orientation to obtain the response of an EAP required for a specific application.

5.2.2. Model 2: Non $\mathcal{A}$-polyconvex constitutive law

In the previous example, we have examined the behaviour of a fibre-reinforced EAP with a constitutive law comprised of $\mathcal{A}$-polyconvex invariants. However, the model does not contain electro-mechanical coupling of the fibres described by invariant $K_2^{\mathcal{D}_{\infty h}}$. The model from the previous section is enhanced as

$$\bar{e}_{\mathcal{D}_{\infty h},2}(\boldsymbol{F}, \boldsymbol{D}_0, \boldsymbol{M}) = \bar{e}_{\mathcal{D}_{\infty h},1}(\boldsymbol{F}, \boldsymbol{D}_0, \boldsymbol{M}) + \frac{1}{2\varepsilon_4} K_2^{\mathcal{D}_{\infty h}}(\boldsymbol{F}, \boldsymbol{D}_0, \boldsymbol{M}). \tag{5.16}$$

Note that coupled electro-mechanical behaviour of fibres is often neglected see, e.g., [24,91].

Since the model contains a non $\mathcal{A}$-polyconvex contribution, it is difficult to prove the $\mathcal{A}$-polyconvex of the model. Therefore, a possible loss of rank-one convexity is investigated for the case with fixed fibre orientation defined by $\boldsymbol{M} = \begin{bmatrix} 1/\sqrt{3} & 1/\sqrt{3} & 1/\sqrt{3} \end{bmatrix}^T$, and material parameter $\varepsilon_4 = 19.2\varepsilon_0$.

The loss of rank-one convexity, i.e., ellipticity can be detected through evaluation of the minors of the acoustic tensor (3.14). However, evaluation of ellipticity loss is computationally demanding and not practical for real three-dimensional simulations. Note that several efficient strategies for the detection of loss of ellipticity have been proposed, see, e.g., [92] and references therein.

It is well known that homogenisation of fibre-reinforced composites with the matrix and fibres described by polyconvex material laws does not generally lead to a polyconvex model at the macroscale, i.e., polyconvexity is not preserved by homogenisation [93,94]. It can be demonstrated that the loss of polyconvexity of fibre-reinforced elastomers has a clear physical meaning of a long wave-length instability [95].

The results of the simulation for three levels of ΔV are shown in Fig. 7. The contour plots display values of the minimal minor of the acoustic tensor normalised by μ_1. The results in case (a) show only positive values of the minor. The value is approaching zero in one element in case (b), and negative values can be detected in case (c), meaning that the rank-one convexity has been lost. The loss of rank-one convexity proves that the proposed energy (5.16) is not $\mathcal{A}$-polyconvex. Even though the loss of rank-one convexity indicates that the governing equations of the electro-mechanical problem become ill-posed and the simulation should be terminated, the evolution of loss of ellipticity is further demonstrated in Fig. 7(d).

5.3. Numerical example 3

The objectives of this example are to:

- Detect the onset of instabilities on a rank-one DE laminated composite square membrane.
- Observe the different buckling patterns in terms of the preferred orientation of transverse isotropy.

The geometry for this numerical example is given by a square membrane of side $l = 0.06$ m and thickness $h = 0.001$ m, clamped along all its side faces, as represented in Fig. 8. The membrane is subjected to a prescribed electric surface charge on its base while grounded to zero potential on its topside. Geometrical and Finite Element simulation parameters are presented in Table 6. $Q3$ Finite Elements are used to interpolate both displacement and electric potential, being 104,188 the total number of degrees of freedom, and the surface charge is applied incrementally, being $\Lambda \in [0, 1]$ the load factor. The two-field variational formulation $\Pi_\Psi(\boldsymbol{\phi}, \varphi)$ in Eq. (2.27) has
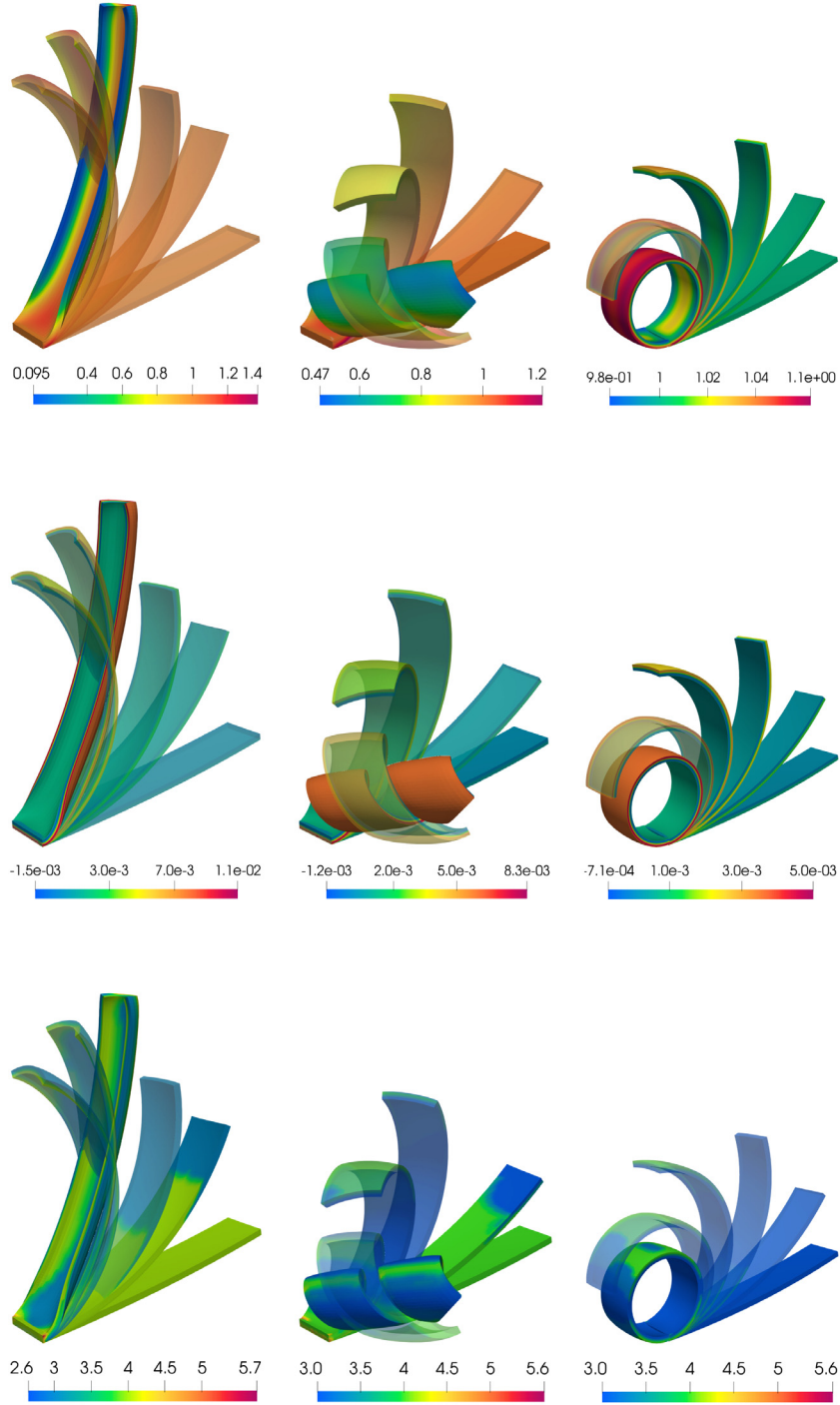
Fig. 6. Deformation of an EAP with different fibre alignment, columns from left to right correspond to $\boldsymbol{M} = \begin{bmatrix} 1 & 0 & 0 \end{bmatrix}^T$, with the snapshots correspond to loading parameter $\Lambda = (0, 10, 15, 30, 60)$; $\boldsymbol{M} = \begin{bmatrix} 1/\sqrt{2} & 1/\sqrt{2} & 0 \end{bmatrix}^T$, $\Lambda = (0, 5, 15, 20, 30, 45)$, and $\boldsymbol{M} = \begin{bmatrix} 0 & 1 & 0 \end{bmatrix}^T$, $\Lambda = (0, 5, 10, 15, 20, 30)$. Contour plots in the first row display deformation gradient component F_{22}, the second row displays electric displacement component D_{03}, and the last row displays the minimal value of minor of acoustic tensor normalised by μ_1.
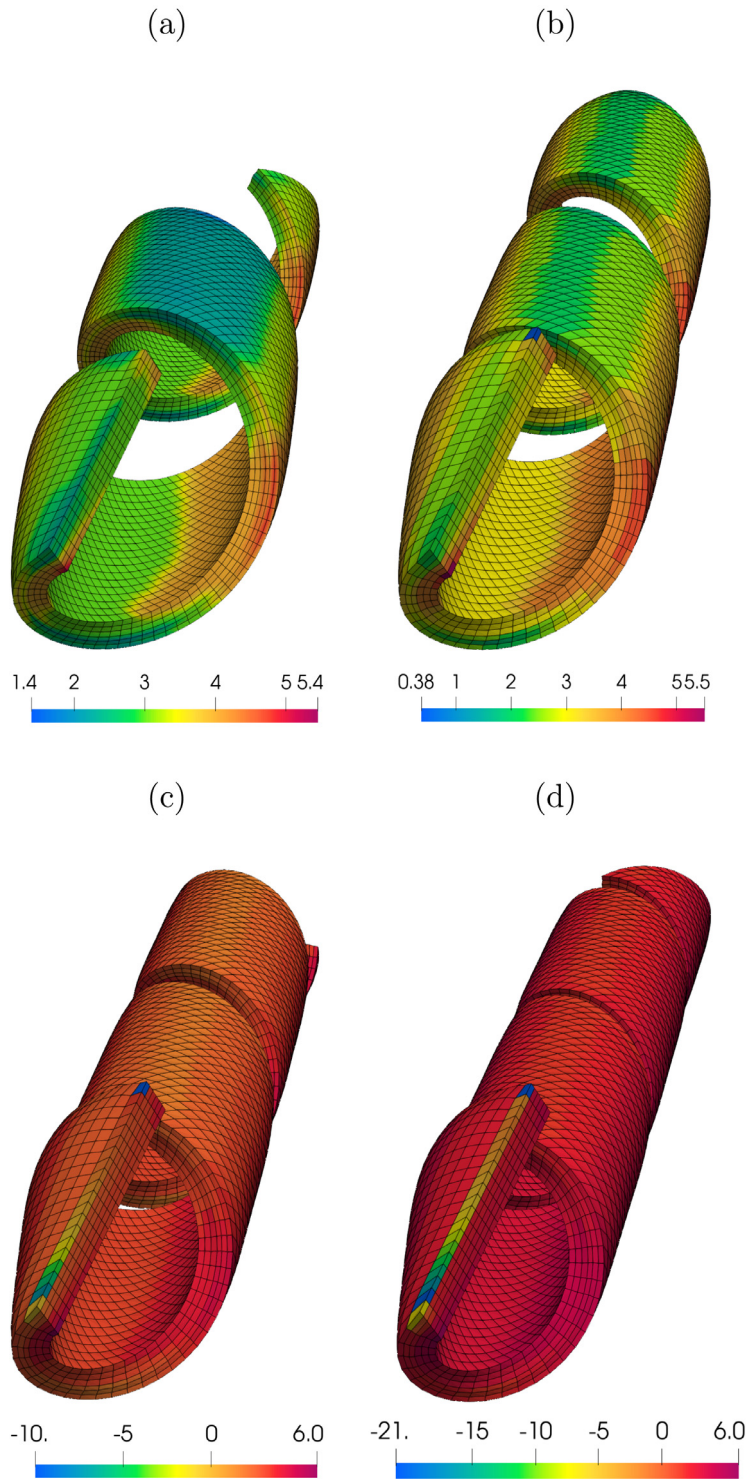
Fig. 7. Deformation of an EAP reinforced with fibres in direction $\boldsymbol{M} = \begin{bmatrix} 1/\sqrt{3} & 1/\sqrt{3} & 1/\sqrt{3} \end{bmatrix}^T$ for four levels of loading parameter, namely, $\Lambda = (40, 44, 47, 49)$. Contour plots display minimal minor of the acoustic tensor normalised by μ_1. The negative value of a minor of the acoustic tensor means that rank-one convexity has been lost.
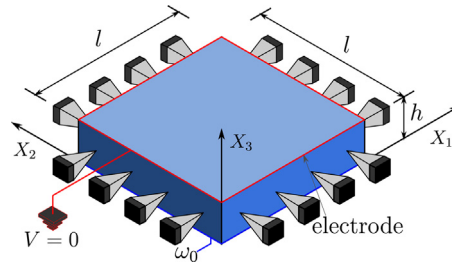
Fig. 8. Numerical example 4. Geometry and boundary conditions.

Table 6
Numerical example 4. Geometrical and simulation parameters.

Geometrical parameters				Simulation parameters		
	l	0.06	m		N_x	60
	h	0.001	m		N_y	60
					N_z	2
Electric charge	ω_0	0.02	C/m^2	Newton tolerance		10^{-6}

Table 7
Material properties for example 3.

μ_1	μ_2	μ_3	λ	ε_1	ε_2	ε_3
1×10^5	$1.0\mu_1$	$1.0\mu_1$	$10^3 \times \mu_1$	$9.6\varepsilon_0$	$2.88\varepsilon_0$	$1.92\varepsilon_0$

been considered using the aforementioned Finite Element discretisation. A volumetric force acting along the positive $0X_3$ axis of value 10, N kg^{-1} is considered.

A similar study was conducted in [96,97], where a squared membrane, made of a rank-one laminated DE, was subjected to electrical stimuli in order to observe the development of instabilities as it deforms. In this work, we consider the transversely isotropic constitutive model given in Eq. (5.15). The material parameters featuring in the model can be found in Table 7.

With regard to the preferred direction M, six values have been considered (see Fig. 9). The electrically induced deformation pattern attained by the elastomeric material is indeed highly influenced by the preferred direction M, as it can be clearly appreciated from Fig. 9. Naturally, this influence is also reflected in the contour plot pressure distribution over the elastomeric material, as shown in Fig. 10.

5.4. Numerical example 4

The objectives of this example are to:

- Demonstrate the influence of the fibre orientation on the deformation of a piezoelectric EAP in the case of twisting in a realistic three-dimensional setting.
- Study the loss of the generalised rank-one convexity.

In the last example, we examine a constitutive law with $\mathcal{C}_\infty$ symmetry, i.e., the symmetry applicable to electroactive materials exhibiting piezoelectric effects. This example includes the twisting of a piezoelectric material whose geometry is characterised in Fig. 11(a). The figure also displays the finite element structured mesh used for the simulation with an element size chosen as $0.25 \times 0.25 \times 0.25$. Note that this example is an extension of the elastic case taken from [75] to electromechanics. The structure is clamped at the bottom, i.e., $Z = 0$, and loaded by pressure follower load $p = 0.45\mu_1$, see 11(b). The electric potential is fixed to zero at the plane defined by $Y = -0.5$.
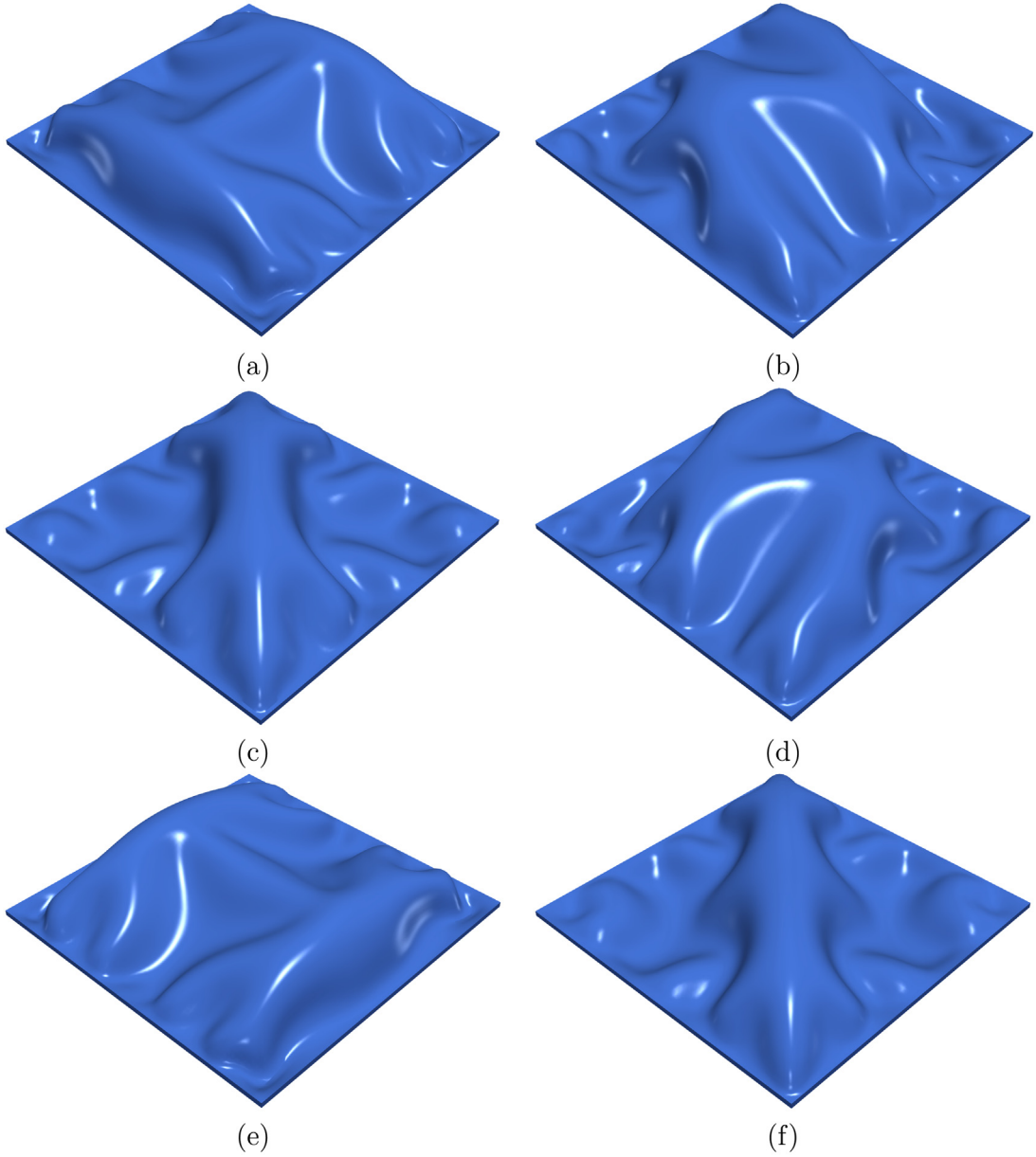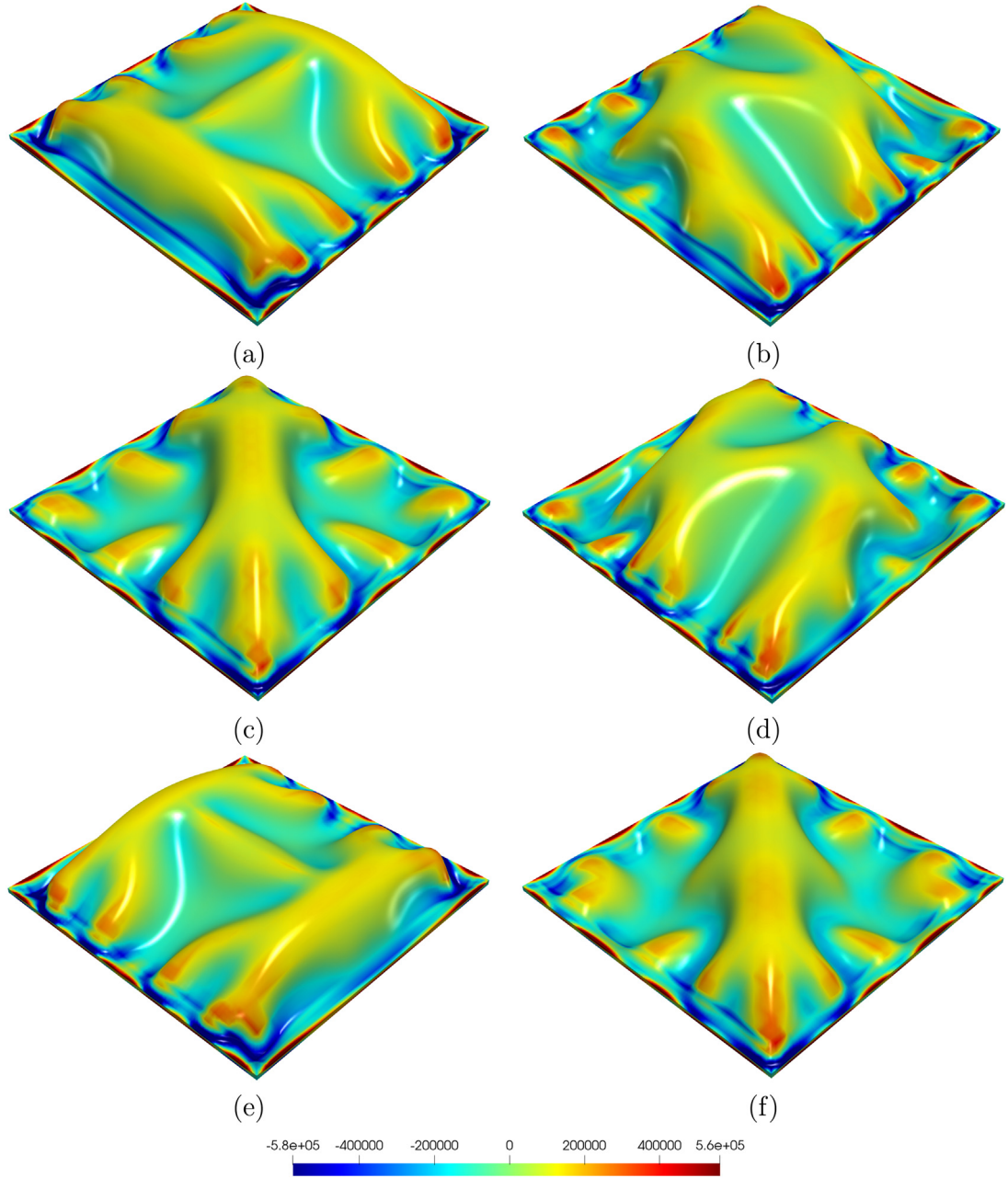
Fig. 9. Electrically induced buckling for numerical example 4 for a value of the accumulated load factor Λ of $\Lambda = 0.4$. Different preferred directions $\boldsymbol{M}$, spherically parametrised according to $\boldsymbol{M} = \begin{bmatrix} \cos\theta\sin(\phi) & \sin\theta\sin(\phi) & \cos(\phi) \end{bmatrix}^T$, with (θ, ϕ): (a) $(0,0)$; (b) $(\pi/8, 0)$; (c) $(\pi/4, 0)$; (d) $(3\pi/8, 0)$; (e) $(\pi/2, 0)$; (f) $(\pi/4, \pi/4)$.

The proposed energy of the material has the form

$$\bar{e}_{\mathcal{C}_\infty}(\boldsymbol{F}, \boldsymbol{D}_0, \boldsymbol{M}) = \bar{e}_1(\boldsymbol{F}) + \bar{e}_2(\boldsymbol{F}, \boldsymbol{M}) + \bar{e}_3(\boldsymbol{F}, \boldsymbol{D}_0) + \bar{e}_{4,\mathcal{C}_\infty}(\boldsymbol{F}, \boldsymbol{D}_0, \boldsymbol{M}), \tag{5.17a}$$

$$\bar{e}_{4,\mathcal{C}_\infty}(\boldsymbol{F}, \boldsymbol{D}_0, \boldsymbol{M}) = \sqrt{\frac{\mu_4}{\varepsilon_4}} \left(K_2^{\mathcal{C}_\infty}(\boldsymbol{F}, \boldsymbol{D}_0, \boldsymbol{M}) - K_1^{\mathcal{C}_\infty}(\boldsymbol{D}_0) \right), \tag{5.17b}$$

-5.8e+05   -400000   -200000   0   200000   400000   5.6e+05

Fig. 10. Electrically induced buckling for numerical example 4 for a value of the accumulated load factor Λ of $\Lambda = 0.4$. Contour plot distribution of hydrostatic pressure $p = \mathrm{tr}(J^{-1} P F^T)$. Different preferred directions M, spherically parametrised according to $M = \begin{bmatrix} \cos\theta\sin(\phi) & \sin\theta\sin(\phi) & \cos(\phi) \end{bmatrix}^T$, with (θ, ϕ): (a) $(0,0)$; (b) $(\pi/8, 0)$; (c) $(\pi/4, 0)$; (d) $(3\pi/8, 0)$; (e) $(\pi/2, 0)$; (f) $(\pi/4, \pi/4)$.

where $K_1^{\mathcal{C}_\infty} = D_0 \cdot M$, and $K_2^{\mathcal{C}_\infty} = d \cdot FM$. The material parameters have been chosen according to Table 8. We already know that invariant $K_2^{\mathcal{C}_\infty}$ is not $\mathcal{A}$-polyconvex; thus, $\mathcal{A}$-polyconvexity of $\bar{e}_{\mathcal{C}_\infty}$ cannot be guaranteed. However, invariant $K_{2,\mathrm{pol}}^{\mathcal{C}_\infty} = \eta^2 I_7 + \psi^2 I_4 + 2\eta\psi K_2^{\mathcal{C}_\infty}$ is $\mathcal{A}$-polyconvex meaning that invariants I_4 and I_7 can compensate for non $\mathcal{A}$-polyconvexity of $K_2^{\mathcal{C}_\infty}$. $\mathcal{A}$-polyconvexity of $\bar{e}_{\mathcal{C}_\infty}$ depends on the relation between material coefficients $\mu_3/2$,

(a)   (b)
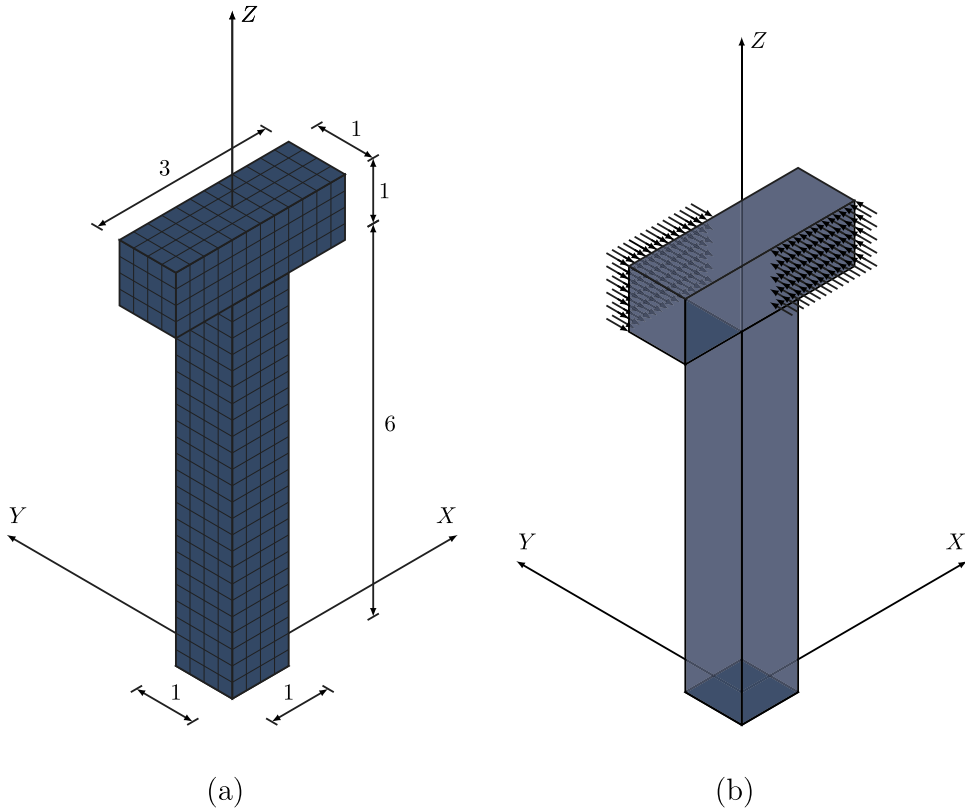
Fig. 11. Example 4. Problem setting.

Table 8
Material properties for example 4.

μ_1	μ_2	μ_3	μ_4	λ	ε_1	ε_2	ε_4	α	β
1×10^9	$1.0\mu_1$	$1.0\mu_1$	$1.0\mu_1$	$10^3 \times \mu_1$	$4.8\varepsilon_0$	$10^6 \times \varepsilon_1$	$10^3 \times \varepsilon_1$	1	1

$1/(2J\varepsilon_1)$, and $\sqrt{\mu_4/\varepsilon_4}$. Combining $\bar{e}_2$, $\bar{e}_3$, and $\bar{e}_{4,\mathcal{C}_\infty}$ leads to

$$\bar{e}_2(\boldsymbol{F}, \boldsymbol{M}) + \bar{e}_3(\boldsymbol{F}, \boldsymbol{D}_0) + \bar{e}_{4,\mathcal{C}_\infty}(\boldsymbol{D}_0) = \left(\frac{\mu_3}{2} - \eta^2\right)(\boldsymbol{FM} \cdot \boldsymbol{FM}) + \left(\frac{1}{2\varepsilon_1 J} - \psi^2\right)(\boldsymbol{FD}_0 \cdot \boldsymbol{FD}_0)$$

$$+ \eta^2(\boldsymbol{FM} \cdot \boldsymbol{FM}) + \psi^2(\boldsymbol{FD}_0 \cdot \boldsymbol{FD}_0) + \sqrt{\frac{\mu_4}{\varepsilon_4}}\boldsymbol{FD}_0 \cdot \boldsymbol{FM}$$

$$- \mu_3 \ln I_3(\boldsymbol{F}) + \frac{1}{2\varepsilon_2} I_6(\boldsymbol{D}_0) - \sqrt{\frac{\mu_4}{\varepsilon_4}} K_1^{\mathcal{C}_\infty}(\boldsymbol{D}_0). \tag{5.18}$$

Clearly, the energy is $\mathcal{A}$-polyconvexity if there exist η and ψ such as the following conditions are satisfied

$$2\eta\psi = \sqrt{\frac{\mu_4}{\varepsilon_4}}, \qquad \frac{\mu_3}{2} \geq \eta^2, \qquad \frac{1}{2\varepsilon_1 J} \geq \psi^2. \tag{5.19}$$

Note that the last condition contains $J \in (0, \infty)$; however, this condition can be satisfied if we restrict to nearly incompressible formulation which is considered in this example. To satisfy the above conditions for the considered material parameters given in Table 8, one can for example choose

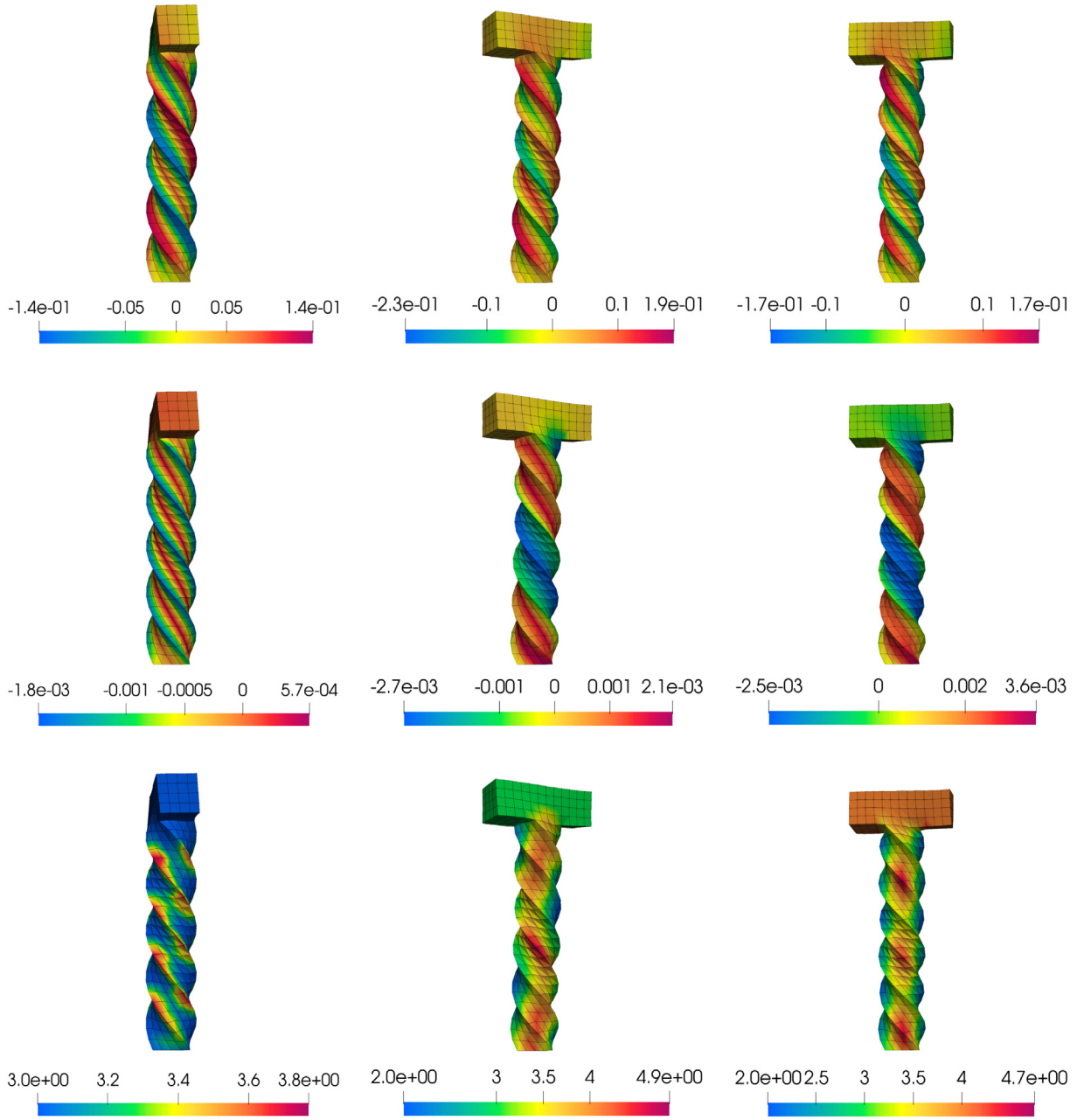$$\eta^2 = \frac{\mu_3}{2}, \quad \psi^2 = \frac{1}{2\varepsilon_4}$$

Fig. 12. Deformation of an EAP with $\mathcal{C}_\infty$ symmetry, i.e., exhibiting piezoelectric effects; columns from left to right correspond to different fibre alignment, namely to $\boldsymbol{M} = \begin{bmatrix} 0 & 0 & 1 \end{bmatrix}^T$; $\boldsymbol{M} = \begin{bmatrix} 1/\sqrt{3} & 1/\sqrt{3} & 1/\sqrt{3} \end{bmatrix}^T$, and $\boldsymbol{M} = \begin{bmatrix} 1/\sqrt{2} & 1/\sqrt{2} & 0 \end{bmatrix}^T$. Contour plots in the first row display deformation gradient component F_{13}, the second row show electric displacement component D_{03}, and the last row display minimal value of minor of acoustic tensor normalised by μ_1.

Fig. 12 displays the contour plots of the deformation gradient component F_{13}, the electric displacement component D_{03}, and the minimal value of minor of acoustic tensor normalised by μ_1 for three different orientations of the fibres, namely $\boldsymbol{M} = \begin{bmatrix} 0 & 0 & 1 \end{bmatrix}^T$; $\boldsymbol{M} = \begin{bmatrix} 1/\sqrt{3} & 1/\sqrt{3} & 1/\sqrt{3} \end{bmatrix}^T$, and $\boldsymbol{M} = \begin{bmatrix} 1/\sqrt{2} & 1/\sqrt{2} & 0 \end{bmatrix}^T$. Note that the calculations were performed using the mixed Hu–Washizu variational principle, see Appendix A.3 for more details.

6. Conclusions

This paper has presented a polyconvex phenomenological invariant-based transversely formulation and computational framework for the simulation of EAPs at large strains. The paper permits the stable in silico simulation at large strains of an internal transversely isotropic crystallographic structure of the selected types $\mathcal{D}_{\infty h}$ and $\mathcal{C}_{\infty}$ [78]. The paper also bridges the gap between the work developed by Šilhavý [62] regarding the existence of minimisers and other key computational requirements, such as, rank-one convexity and ellipticity [57], the latter necessary to prevent the appearance of spurious mesh-dependent results.

Four numerical examples are included in order to demonstrate the effect that the anisotropic orientation and the contrast of material properties, as well as the level of deformation and electric field, have upon the response of the EAP when subjected to large three-dimensional stretching, bending, and torsion, including the possible development of wrinkling. Whilst the first example focuses on an academic type of problem, that is, homogeneous deformation, the latter three explore the use of Finite Element discretisations to monitor the response of the framework in realistic three-dimensional in-silico simulations. This manuscript paves the way towards the in-silico simulation of novel soft robotics components made up of predominantly dominant transversely isotropic Electro-Active Polymers (EAPs). Crucially, this type of phenomenologically based model can be enhanced and informed via the use of laboratory data experiments, the up-scaling of computational homogenisation of complex micro-architecture EAPs, or even the use of Artificial Intelligence type of approaches. These will be the focus of our future work.

Declaration of competing interest

The authors declare that they have no known competing financial interests or personal relationships that could have appeared to influence the work reported in this paper.

Data availability

The authors are unable or have chosen not to specify which data has been used.

Acknowledgements

Appendix

A.1. Ellipticity and acoustic tensor

As shown in [58], the unknown fields $\boldsymbol{\phi}$ and $\boldsymbol{D}_0$ can be written as a perturbation with respect to equilibrium states $\boldsymbol{\phi}^{\text{eq}}$ and $\boldsymbol{D}_0^{\text{eq}}$, respectively, by means of the addition of transient travelling (plane) wave functions as

$$\boldsymbol{\phi} = \boldsymbol{\phi}^{\text{eq}} + \boldsymbol{u} f(\alpha); \qquad \boldsymbol{D}_0 = \boldsymbol{D}_0^{\text{eq}} + \boldsymbol{V}_\perp g(\alpha); \qquad \alpha = \boldsymbol{X} \cdot \boldsymbol{V} - ct, \tag{A.1}$$

where $\boldsymbol{V}$ represents the polarisation vector of the travelling wave, c the associated speed of propagation of the perturbation with amplitudes $\boldsymbol{u}$ and $\boldsymbol{V}_\perp$ and f and g two arbitrary α-scalar functions. Substitution of above ansatz into (2.1) and (2.6a), respectively, results in

$$\boldsymbol{F} = \underbrace{\nabla_0 \boldsymbol{\phi}^{\text{eq}}}_{=\boldsymbol{F}^{\text{eq}}} + (\boldsymbol{u} \otimes \boldsymbol{V}) f'(\alpha); \tag{A.2a}$$

$$\text{DIV}\boldsymbol{D}_0 - \rho_0 = \underbrace{\text{DIV}\boldsymbol{D}_0^{\text{eq}} - \rho_0}_{=0} + (\boldsymbol{V}_\perp \cdot \boldsymbol{V}) \, g'(\alpha) = 0, \tag{A.2b}$$

hence, $V_\perp$ must be orthogonal to V. Linearisation of the first Piola–Kirchhoff stress tensor P and the electric field E_0 about equilibrium states $P^{\text{eq}} = P(\mathcal{U}^{\text{eq}})$ and $E_0^{\text{eq}} = E_0(\mathcal{U}^{\text{eq}})$, with $\mathcal{U}^{\text{eq}} = (F^{\text{eq}}, D_0^{\text{eq}})$, gives

$$\begin{bmatrix} P \\ E_0 \end{bmatrix} = \begin{bmatrix} P^{\text{eq}} \\ E_0^{\text{eq}} \end{bmatrix} + \begin{bmatrix} \mathcal{C}_e & \mathcal{Q}^T \\ \mathcal{Q} & \boldsymbol{\theta} \end{bmatrix} \begin{bmatrix} : (u \otimes V) f'(\alpha) \\ V_\perp g(\alpha) \end{bmatrix}. \tag{A.3}$$

Substitution of (A.3) into (2.3) and into Faraday's law (2.5a)[11] gives

$$\text{DIV} P + b_0 = \underbrace{\text{DIV} P^{\text{eq}} + b_0}_{=0} + \underbrace{\mathcal{C}_{e,VV} \, u f''(\alpha) + \mathcal{Q}_V^T V_\perp g'(\alpha)}_{\rho_R c^2 u f''(\alpha)}; \tag{A.4a}$$

$$\text{CURL} E_0 = \underbrace{\text{CURL} E_0^{\text{eq}}}_{=0} + \mathcal{E}_{\mathcal{V}} \left[\mathcal{Q}_V \, u f''(\alpha) + \boldsymbol{\theta} \, V_\perp g'(\alpha) \right] = 0, \tag{A.4b}$$

where

$$\left[\mathcal{C}_{e,VV} \right]_{ij} = \mathcal{C}_{e,iIjJ} V_I V_J, \qquad [\mathcal{Q}_V]_{Ij} = \mathcal{Q}_{IjJ} V_J, \qquad [\mathcal{E}_{\mathcal{V}}]_{IJ} = \mathcal{E}_{IJK} V_K, \tag{A.5}$$

where $\mathcal{E}_{IJK}$ denotes the Levi-Civita third-order tensor. Notice that the last underbraced term on the right-hand side of (A.4a) is identified with the inertial term corresponding to the acceleration effect with ρ_R the density of the electroactive material. Naturally, a satisfaction of (A.4b) requires the vector within squared brackets to be collinear to V, which permits to obtain

$$V_\perp g'(\alpha) = \boldsymbol{\theta}^{-1} \left[\beta_V V - \mathcal{Q}_V \, u f''(\alpha) \right] \tag{A.6}$$

with β_V a proportionality constant, which can be easily computed from (A.6) by projecting both sides of the equation against V, rendering

$$\beta_V = \frac{V \cdot \left(\boldsymbol{\theta}^{-1} \mathcal{Q}_V \right) u}{V \cdot \boldsymbol{\theta}^{-1} V} f''(\alpha). \tag{A.7}$$

Substitution of (A.7) into (A.6) and after some algebraic manipulation gives

$$V_\perp g'(\alpha) = \boldsymbol{\theta}^{-1} \Omega \mathcal{Q}_V f''(\alpha); \qquad \Omega = \left[\frac{V \otimes \boldsymbol{\theta}^{-1} V}{V \cdot \boldsymbol{\theta}^{-1} V} - I \right]. \tag{A.8}$$

Substitutions of Eq. (A.8) into (A.4a), results in

$$Qu = \rho c^2 u; \qquad Q = \mathcal{C}_{e,VV} + \mathcal{Q}_V^T \boldsymbol{\theta}^{-1} \Omega \mathcal{Q}_V, \tag{A.9}$$

where Q is the so-called electro-mechanical acoustic tensor which is a function of the constitutive tensors $\mathcal{C}_e$, $\mathcal{Q}$, $\boldsymbol{\theta}$ (dependent upon the state of electro-deformation), as well as the polarisation orientation V. A reasonable physical requirement is that of the existence of real wave speeds, which requires the positive semi-definiteness of the acoustic tensor Q, that is,

$$u \cdot Qu \geq 0; \qquad \forall \mathcal{U}, u, V. \tag{A.10}$$

A.2. Polyconvex invariants

A.2.1. Proof of polyconvexity of I_8^{pol}

The purpose here is prove that invariant I_8^{pol} is convex with respect to H and D_0. For that, let us compute $D^2 I_8^{\text{pol}}[\delta H, \delta D_0; \delta H, \delta D_0]$, i.e.

$$\begin{aligned} D^2 I_8^{\text{pol}}[\delta H, \delta D_0; \delta H, \delta D_0] = {} & 4\alpha^2 ||H||^2 ||\delta H||^2 + 8\alpha^2 (H : \delta H)^2 \\ & + 2\alpha\beta ||\delta H D_0 + H \delta D_0||^2 + 4\alpha\beta H D_0 \cdot \delta H \delta D_0 \\ & + 4\beta^2 ||D_0||^2 ||\delta D_0||^2 + 8\beta^2 (D_0 \cdot \delta D_0)^2 \\ & \geq 4\alpha^2 ||H||^2 ||\delta H||^2 + 4\alpha\beta H D_0 \cdot \delta H \delta D_0 + 4\beta^2 ||D_0||^2 ||\delta D_0||^2 \end{aligned} \tag{A.11}$$

---

[11] In this case, use is made of the more generic expression for Faraday's law, namely $\text{CURL} E_0 = 0$.

Application of the Cauchy–Schwarz inequality in the previous equation yields

$$D^2 I_8^{\text{pol}}[\delta \boldsymbol{H}, \delta \boldsymbol{D}_0; \delta \boldsymbol{H}, \delta \boldsymbol{D}_0] \geq 4\left(\alpha^2 ||\boldsymbol{H}||^2 ||\delta \boldsymbol{H}||^2 - \alpha\beta ||\boldsymbol{H}\boldsymbol{D}_0|| ||\delta \boldsymbol{H}\delta \boldsymbol{D}_0|| + \beta^2 ||\boldsymbol{D}_0||^2 ||\delta \boldsymbol{D}_0||^2\right) \tag{A.12}$$

and by definition, the norm of a matrix $\boldsymbol{H}$ verifies that

$$||\boldsymbol{H}\boldsymbol{v}|| \leq ||\boldsymbol{H}|| ||\boldsymbol{v}|| \tag{A.13}$$

for any vector $\boldsymbol{v}$. Therefore, it is possible to conclude that

$$\begin{aligned}
D^2 I_8^{\text{pol}}[\delta \boldsymbol{H}, \delta \boldsymbol{D}_0; \delta \boldsymbol{H}, \delta \boldsymbol{D}_0] &\geq 4\left(\alpha^2 ||\boldsymbol{H}||^2 ||\delta \boldsymbol{H}||^2 - \alpha\beta ||\boldsymbol{H}|| ||\boldsymbol{D}_0|| ||\delta \boldsymbol{H}|| ||\delta \boldsymbol{D}_0|| + \beta^2 ||\boldsymbol{D}_0||^2 ||\delta \boldsymbol{D}_0||^2\right) \\
&\geq 4\left(\alpha^2 ||\boldsymbol{H}||^2 ||\delta \boldsymbol{H}||^2 - 2\alpha\beta ||\boldsymbol{H}|| ||\boldsymbol{D}_0|| ||\delta \boldsymbol{H}|| ||\delta \boldsymbol{D}_0|| + \beta^2 ||\boldsymbol{D}_0||^2 ||\delta \boldsymbol{D}_0||^2\right) \\
&= 4\left(\alpha ||\boldsymbol{H}|| ||\delta \boldsymbol{H}|| - \beta ||\boldsymbol{D}_0|| ||\delta \boldsymbol{D}_0||\right)^2 \geq 0
\end{aligned} \tag{A.14}$$

which therefore, concludes the proof.

A.2.2. Proof of polyconvexity of $\widetilde{K}_{2_{pol}}^{\mathcal{D}_{\infty h}}$

The purpose here is prove that invariant $\widetilde{K}_{2_{\text{pol}}}^{\mathcal{D}_{\infty h}}$ is convex with respect to $\boldsymbol{d}$ and $\boldsymbol{F}$. For that, let us compute $D^2 \widetilde{K}_{2_{\text{pol}}}^{\mathcal{D}_{\infty h}}[\delta \boldsymbol{d}, \delta \boldsymbol{F}; \delta \boldsymbol{d}, \delta \boldsymbol{F}]$, i.e.

$$\begin{aligned}
D^2 \widetilde{K}_{2_{\text{pol}}}^{\mathcal{D}_{\infty h}}[\delta \boldsymbol{d}, \delta \boldsymbol{F}; \delta \boldsymbol{d}, \delta \boldsymbol{F}] &= 4\alpha^2 ||\boldsymbol{d}||^2 ||\delta \boldsymbol{d}||^2 + 8\alpha^2 (\boldsymbol{d} \cdot \delta \boldsymbol{d})^2 \\
&\quad + 2\alpha\beta (\delta \boldsymbol{d} \cdot \boldsymbol{F}\boldsymbol{M} + \boldsymbol{d} \cdot \delta \boldsymbol{F}\boldsymbol{M})^2 + 4\alpha\beta ((\boldsymbol{d} \cdot \boldsymbol{F}\boldsymbol{M})(\delta \boldsymbol{d} \cdot \delta \boldsymbol{F}\boldsymbol{M})) \\
&\quad + 4\beta^2 ||\boldsymbol{F}\boldsymbol{M}||^2 ||\delta \boldsymbol{F}\boldsymbol{M}||^2 + 8\beta^2 (\boldsymbol{F}\boldsymbol{M} \cdot \delta \boldsymbol{F}\boldsymbol{M})^2 \\
&\geq 4\alpha^2 ||\boldsymbol{d}||^2 ||\delta \boldsymbol{d}||^2 + 4\alpha\beta ((\boldsymbol{d} \cdot \boldsymbol{F}\boldsymbol{M})(\delta \boldsymbol{d} \cdot \delta \boldsymbol{F}\boldsymbol{M})) + 4\beta^2 ||\boldsymbol{F}\boldsymbol{M}||^2 ||\delta \boldsymbol{F}\boldsymbol{M}||^2
\end{aligned} \tag{A.15}$$

Application of the Cauchy–Schwarz inequality in the previous equation yields

$$D^2 \widetilde{K}_{2_{\text{pol}}}^{\mathcal{D}_{\infty h}}[\delta \boldsymbol{d}, \delta \boldsymbol{F}; \delta \boldsymbol{d}, \delta \boldsymbol{F}] \geq 4\left(\alpha^2 ||\boldsymbol{d}||^2 ||\delta \boldsymbol{d}||^2 - \alpha\beta ||\boldsymbol{d}|| ||\delta \boldsymbol{d}|| ||\boldsymbol{F}\boldsymbol{M}|| ||\delta \boldsymbol{F}\boldsymbol{M}|| + \beta^2 ||\boldsymbol{F}\boldsymbol{M}||^2 ||\delta \boldsymbol{F}\boldsymbol{M}||^2\right) \tag{A.16}$$

Therefore, it is possible to conclude that

$$\begin{aligned}
D^2 \widetilde{K}_{2_{\text{pol}}}^{\mathcal{D}_{\infty h}}[\delta \boldsymbol{d}, \delta \boldsymbol{F}; \delta \boldsymbol{d}, \delta \boldsymbol{F}] &\geq 4\left(\alpha^2 ||\boldsymbol{d}||^2 ||\delta \boldsymbol{d}||^2 - \alpha\beta ||\boldsymbol{H}|| ||\boldsymbol{D}_0|| ||\delta \boldsymbol{H}|| ||\delta \boldsymbol{D}_0|| + \beta^2 ||\boldsymbol{F}\boldsymbol{M}||^2 ||\delta \boldsymbol{F}\boldsymbol{M}||^2\right) \\
&\geq 4\left(\alpha^2 ||\boldsymbol{d}||^2 ||\delta \boldsymbol{d}||^2 - 2\alpha\beta ||\boldsymbol{H}|| ||\boldsymbol{D}_0|| ||\delta \boldsymbol{H}|| ||\delta \boldsymbol{D}_0|| + \beta^2 ||\boldsymbol{F}\boldsymbol{M}||^2 ||\delta \boldsymbol{F}\boldsymbol{M}||^2\right) \\
&= 4\left(\alpha ||\boldsymbol{d}|| ||\delta \boldsymbol{d}|| - \beta ||\boldsymbol{F}\boldsymbol{M}|| ||\delta \boldsymbol{F}\boldsymbol{M}||\right)^2 \geq 0
\end{aligned} \tag{A.17}$$

which therefore, concludes the proof.

A.2.3. Proof of polyconvexity of $K_{2,pol}^{\mathcal{C}_\infty}$

The purpose here is prove that invariant $K_{2,\text{pol}}^{\mathcal{C}_\infty}$ is convex with respect to $\boldsymbol{d}$ and $\boldsymbol{F}_0$. For that, let us compute $D^2 K_{2,\text{pol}}^{\mathcal{C}_\infty}[\delta \boldsymbol{d}, \delta \boldsymbol{F}; \delta \boldsymbol{d}, \delta \boldsymbol{F}]$, i.e.

$$\begin{aligned}
D^2 K_{2,\text{pol}}^{\mathcal{C}_\infty}[\delta \boldsymbol{d}, \delta \boldsymbol{F}; \delta \boldsymbol{d}, \delta \boldsymbol{F}] &= 2\eta^2 ||\delta \boldsymbol{d}||^2 + 4\eta\psi (\delta \boldsymbol{d} \cdot \delta \boldsymbol{F}\boldsymbol{M}) + 2\psi^2 ||\delta \boldsymbol{F}\boldsymbol{M}||^2 \\
&= 2||\eta \delta \boldsymbol{d} + \psi \delta \boldsymbol{F}\boldsymbol{M}||^2 \geq 0
\end{aligned} \tag{A.18}$$

which therefore, concludes the proof.

A.3. Finite element implementation

This Appendix briefly summarises the Finite Element spatial discretisation procedure implemented for the second and third numerical examples. Specifically, we focused on the mixed Hu–Washizu type of variational principle $\tilde{\Pi}_e$ (2.22), whose stationary conditions yield

$$D\tilde{\Pi}_e[\delta\boldsymbol{\phi}] = \int_{\Omega_0} \partial e_{\boldsymbol{F}} : \boldsymbol{\nabla}_0 \delta\boldsymbol{\phi} \, dV - D\Pi_{\text{ext}}[\delta\boldsymbol{\phi}] = 0;$$

$$D\tilde{\Pi}_e[\delta\boldsymbol{D}_0] = \int_{\Omega_0} (\partial e_{\boldsymbol{D}_0} + \boldsymbol{\nabla}_0 \varphi) \cdot \delta\boldsymbol{D}_0 \, dV = 0; \tag{A.19}$$

$$D\tilde{\Pi}_e[\delta\varphi] = \int_{\Omega_0} \boldsymbol{D}_0 \cdot \boldsymbol{\nabla}_0 \delta\varphi \, dV - D\Pi_{\text{ext}}[\delta\varphi] = 0,$$

where $\{\boldsymbol{\phi}, \boldsymbol{D}_0, \varphi\} \in \mathbb{V}_{\bar{\boldsymbol{\phi}}}^{\boldsymbol{\phi}} \times \mathbb{V}^{\boldsymbol{D}_0} \times \mathbb{V}_{\bar{\varphi}}^{\varphi}$ and with admissible variations $\{\delta\boldsymbol{\phi}, \delta\boldsymbol{D}_0, \delta\varphi\} \in \mathbb{V}_{\boldsymbol{0}}^{\boldsymbol{\phi}} \times \mathbb{V}^{\boldsymbol{D}_0} \times \mathbb{V}_0^{\varphi}$, defined as

$$\mathbb{V}_{\bar{\boldsymbol{\phi}}}^{\boldsymbol{\phi}} = \left\{ \boldsymbol{\phi} : \Omega_0 \to \mathbb{R}^3; \; [\boldsymbol{\phi}]_i \in H^1(\Omega_0); \; J > 0; \; ; \; | \; \boldsymbol{\phi} = \bar{\boldsymbol{\phi}} \text{ on } \partial\Omega_0^u \right\};$$

$$\mathbb{V}_{\bar{\varphi}}^{\varphi} = \left\{ \varphi : \Omega_0 \to \mathbb{R}; \; \varphi \in H^1(\Omega_0); | \; \varphi = \bar{\varphi} \text{ on } \partial\Omega_0^{\varphi} \right\};$$

$$\mathbb{V}^{\boldsymbol{D}_0} = \left\{ \boldsymbol{D}_0 : \Omega_0 \to \mathbb{R}^3; \; \boldsymbol{D}_0 \in L_2(\Omega_0) \right\}.$$

Further, we apply standard isoparametric Finite Elements and the domain Ω_0 is divided into elements and the displacement, electric potential and electric displacement fields are approximated by means of approximation finite element spaces $\mathbb{V}_{\bar{\boldsymbol{\phi}},h}^{\boldsymbol{\phi}} \subset \mathbb{V}_{\bar{\boldsymbol{\phi}}}^{\boldsymbol{\phi}}$, $V_{\bar{\varphi},h}^{\varphi} \subset V_{\bar{\varphi}}^{\varphi}$, and $V_h^{\boldsymbol{D}_0} \subset V^{\boldsymbol{D}_0}$ defined as

$$\mathbb{V}_{\bar{\boldsymbol{\phi}},h}^{\boldsymbol{\phi}} = \left\{ \boldsymbol{\phi} : \Omega_0 \to \mathbb{R}^3; \; \boldsymbol{\phi} = \sum_{a=1}^{n_{nod}^{\boldsymbol{\phi}}} N_{\boldsymbol{\phi}}^a \boldsymbol{d}_{\boldsymbol{\phi}}^a; | \; \boldsymbol{\phi} = \bar{\boldsymbol{\phi}} \text{ on } \partial\Omega_0^u \right\};$$

$$V_{\bar{\varphi},h}^{\varphi} = \left\{ \varphi : \Omega_0 \to \mathbb{R}^3; \; \varphi = \sum_{a=1}^{n_{nod}^{\varphi}} N_{\varphi}^a d_{\varphi}^a; | \; \varphi = \bar{\varphi} \text{ on } \partial\Omega_0^{\varphi} \right\};$$

$$V_h^{\boldsymbol{D}_0} = \left\{ \boldsymbol{D}_0 : \Omega_0 \to \mathbb{R}^3; \; \boldsymbol{D}_0 = \sum_{a=1}^{n_{nod}^{D}} N_{\boldsymbol{D}_0}^a \boldsymbol{d}_{\boldsymbol{D}_0}^a \right\},$$

where for any field $i = \{\boldsymbol{\phi}, \boldsymbol{D}_0, \varphi\}$, n_{nod}^i denotes number of interconnected nodes, N_i^a is the ath basis function and $\boldsymbol{d}_i^a$ is the ath node associated with the appropriate field. Use of above Finite Element interpolation spaces into (A.19) leads to a system of nonlinear algebraic equations, whose solution is obtained via a consistent Newton–Raphson linearisation iterative procedure. In order to reduce the computational cost of the proposed formulation, a piecewise discontinuous interpolation of the field $\boldsymbol{D}_0$ is followed. A standard static condensation procedure [81] is used to condense out the degrees of freedom of the field $\boldsymbol{D}_0$, yielding a formulation with a cost comparable to that of a two-field $(\boldsymbol{\phi}, \varphi)$ formulation.

References

[1] Y. Bar-Cohen, EAP History, Current Status, and Infrastructure in Y. Bar-Cohen, Electroactive Polymer (EAP) Actuators as Artificial Muscles, SPIE Press, 2001, pp. 3–44, chapter 1.

[2] R.D. Kornbluh, R. Pelrine, Q. Pei, S. Oh, J. Joseph, Ultrahigh strain response of field-actuated elastomeric polymers, in: Y. Bar-Cohen (Ed.), Smart Structures and Materials 2000: Electroactive Polymer Actuators and Devices (EAPAD), SPIE, 2000.

[3] R.E. Pelrine, Review of artificial muscle approaches, in: Third Internationat Symposium on Micro Machine and Human Science, 1992.

[4] G. deBotton, L. Tevet-Deree, E.A. Socolsky, Electroactive heterogeneous polymers: Analysis and applications to laminated composites, Mech. Adv. Mater. Struct. 14 (1) (2007) 13–22.

[5] R.E. Pelrine, R.D. Kornbluh, J.P. Joseph, Electrostriction of polymer dielectrics with compliant electrodes as a means of actuation, Sensors Actuators A 64 (1) (1998) 77–85.

[6] R. Pelrine, High-speed electrically actuated elastomers with strain greater than 100%, Science 287 (5454) (2000) 836–839.

[7] S.P. Lacour, H. Prahlad, R. Pelrine, S. Wagner, Mechatronic system of dielectric elastomer actuators addressed by thin film photoconductors on plastic, Sensors Actuators A 111 (2–3) (2004) 288–292.

[8] L. An, F. Wang, S. Cheng, T. Lu, T. Wang, Experimental investigation of the electromechanical phase transition in a dielectric elastomer tube, Smart Mater. Struct. 24 (3) (2015) 035006.

[9] Y. Bar-Cohen, Electroactive polymers (EAP) as actuators for potential future planetary mechanisms, in: Proceedings. NASA/DoD Conference on Evolvable Hardware, 2004, IEEE, 2004.

[10] E. Bortot, R. Denzer, A. Menzel, M. Gei, Analysis of viscoelastic soft dielectric elastomer generators operating in an electrical circuit, Int. J. Solids Struct. 78–79 (2016) 205–215.

[11] F. Carpi, G. Frediani, S. Turco, D. De Rossi, Bioinspired tunable lens with muscle-like electroactive elastomers, Adv. Funct. Mater. 21 (21) (2011) 4152–4158.

[12] A. O'Halloran, F. O'Malley, P. McHugh, A review on dielectric elastomer actuators, technology, applications, and challenges, J. Appl. Phys. 104 (7) (2008) 071101.

[13] F. Carpi, D. De Rossi, R. Kornbluh, R. Pelrine, P. Sommer-Larsen, Dielectric Elastomers as Electromechanical Transducers, Elsevier, 2008.

[14] S. Rudykh, K. Bhattacharya, G. deBotton, Snap-through actuation of thick-wall electroactive balloons, Int. J. Non Linear Mech. 47 (2) (2012) 206–209.

[15] T. Li, C. Keplinger, R. Baumgartner, S. Bauer, W. Yang, Z. Suo, Giant voltage-induced deformation in dielectric elastomers near the verge of snap-through instability, J. Mech. Phys. Solids 61 (2) (2013) 611–628.

[16] T. McKay, B. O'Brien, E. Calius, I. Anderson, An integrated, self-priming dielectric elastomer generator, Appl. Phys. Lett. 97 (6) (2010) 062911.

[17] R.D. Kornbluh, R. Pelrine, H. Prahlad, A. Wong-Foy, B. McCoy, S. Kim, J. Eckerle, T. Low, From boots to buoys: promises and challenges of dielectric elastomer energy harvesting, in: Y. Bar-Cohen, F. Carpi (Eds.), Electroactive Polymer Actuators and Devices (EAPAD) 2011, SPIE, 2011.

[18] M. Aschwanden, A. Stemmer, Polymeric, electrically tunable diffraction grating based on artificial muscles, Opt. Lett. 31 (17) (2006) 2610–2612.

[19] S. Rosset, H.R. Shea, Small, fast, and tough: Shrinking down integrated elastomer transducers, Appl. Phys. Rev. 3 (3) (2016) 031105.

[20] K. Bertoldi, M. Gei, Instabilities in multilayered soft dielectrics, J. Mech. Phys. Solids 59 (1) (2011) 18–42.

[21] R. Xiao, X. Gou, W. Chen, Suppression of electromechanical instability in fiber-reinforced dielectric elastomers, AIP Adv. 6 (3) (2016) 035321.

[22] J. Huang, T. Lu, J. Zhu, D.R. Clarke, Z. Suo, Large, uni-directional actuation in dielectric elastomers achieved by fiber stiffening, Appl. Phys. Lett. 100 (21) (2012) 211901.

[23] L. He, J. Lou, J. Du, Voltage-driven torsion of electroactive thick tubes reinforced with helical fibers, Acta Mech. 229 (5) (2018) 2117–2131.

[24] A. Ahmadi, M. Asgari, Nonlinear coupled electro-mechanical behavior of a novel anisotropic fiber-reinforced dielectric elastomer, Int. J. Non-Linear Mech. 119 (2020) 103364.

[25] Q.M. Zhang, H. Li, M. Poh, F. Xia, Z.-Y. Cheng, H. Xu, C. Huang, An all-organic composite actuator material with a high dielectric constant, Nature 419 (6904) (2002) 284–287.

[26] C. Huang, Q.M. Zhang, G. deBotton, K. Bhattacharya, All-organic dielectric-percolative three-component composite materials with high electromechanical response, Appl. Phys. Lett. 84 (22) (2004) 4391–4393.

[27] C. Huang, Q. Zhang, Enhanced dielectric and electromechanical responses in high dielectric constant all-polymer percolative composites, Adv. Funct. Mater. 14 (5) (2004) 501–506.

[28] P. Ponte Castañeda, M. Siboni, A finite-strain constitutive theory for electro-active polymer composites via homogenization, Int. J. Non Linear Mech. 47 (2) (2012) 293–306.

[29] A. Goshkoderia, S. Rudykh, Electromechanical macroscopic instabilities in soft dielectric elastomer composites with periodic microstructures, Eur. J. Mech. A Solids 65 (2017) 243–256.

[30] H. Stoyanov, M. Kollosche, S. Risse, D.N. McCarthy, G. Kofod, Elastic block copolymer nanocomposites with controlled interfacial interactions for artificial muscles with direct voltage control, Soft Matter 7 (1) (2011) 194–202.

[31] P.I. Galich, S. Rudykh, Shear wave propagation and band gaps in finitely deformed dielectric elastomer laminates: Long wave estimates and exact solution, J. Appl. Mech. 84 (9) (2017).

[32] J. Li, Exchange coupling in P(VDF-TrFE) copolymer based all-organic composites with giant electrostriction, Phys. Rev. Lett. 90 (21) (2003).

[33] J.Y. Li, C. Huang, Q. Zhang, Enhanced electromechanical properties in all-polymer percolative composites, Appl. Phys. Lett. 84 (16) (2004) 3124–3126.

[34] G. deBotton, L. Tevet-Deree, Electroactive polymer composites: analysis and simulation, in: W.D. Armstrong (Ed.), Smart Structures and Materials 2006: Active Materials: Behavior and Mechanics, SPIE, 2006.

[35] L. Tian, L. Tevet-Deree, G. deBotton, K. Bhattacharya, Dielectric elastomer composites, J. Mech. Phys. Solids 60 (1) (2012) 181–198.

[36] M. Gei, K.C. Mutasa, Optimisation of hierarchical dielectric elastomer laminated composites, Int. J. Non Linear Mech. 106 (2018) 266–273.

[37] M. Gei, R. Springhetti, E. Bortot, Performance of soft dielectric laminated composites, Smart Mater. Struct. 22 (10) (2013) 104014.

[38] S. Rudykh, G. deBotton, Stability of anisotropic electroactive polymers with application to layered media, Z. Angew. Math. Phys. 62 (6) (2011) 1131–1142.

[39] R. Toupin, The elastic dielectric, Indiana Univ. Math. J. (ISSN: 0022-2518) 5 (1956) 849–915.

[40] R.A. Toupin, Stress tensors in elastic dielectrics, Arch. Ration. Mech. Anal. 5 (1) (1960) 440–452.

[41] A. Dorfmann, R.W. Ogden, Nonlinear electroelasticity, Acta Mech. 174 (3–4) (2005) 167–183.

[42] A. Dorfmann, R.W. Ogden, Nonlinear electroelastic deformations, J. Elast. 82 (2) (2006) 99–127.

[43] R.M. McMeeking, C.M. Landis, Electrostatic forces and stored energy for deformable dielectric materials, J. Appl. Mech. 72 (4) (2004) 581–590.

[44] Z. Suo, X. Zhao, W. Greene, A nonlinear field theory of deformable dielectrics, J. Mech. Phys. Solids 56 (2) (2008) 467–486.

[45] L. Dorfmann, R. Ogden, Nonlinear Theory of Electroelastic and Magnetoelastic Interactions, Springer, New York, 2014.

[46] C.M. Landis, New finite element formulation for electromechanics, in: Smart Structures and Materials 2002: Active Materials: Behavior and Mechanics, Vol. 4699, International Society for Optics and Photonics, 2002, pp. 31–39.

[47] D. Vu, P. Steinmann, G. Possart, Numerical modelling of non-linear electroelasticity, Internat. J. Numer. Methods Engrg. 70 (6) (2007) 685–704.

[48] D. Vu, P. Steinmann, A 2-D coupled BEM–FEM simulation of electro-elastostatics at large strain, Comput. Methods Appl. Mech. Engrg. 199 (17–20) (2010) 1124–1133.

[49] D. Vu, P. Steinmann, On 3-D coupled BEM–FEM simulation of nonlinear electro-elastostatics, Comput. Methods Appl. Mech. Engrg. 201–204 (2012) 82–90.

[50] M. Jabareen, On the modeling of electromechanical coupling in electroactive polymers using the mixed finite element formulation, Procedia IUTAM 12 (2015) 105–115.

[51] M. Franke, R. Ortigosa, A. Janz, A. Gil, P. Betsch, A mixed variational framework for the design of energy–momentum integration schemes based on convex multi-variable electro-elastodynamics, Comput. Methods Appl. Mech. Engrg. 351 (2019) 109–152.

[52] D. Bishara, M. Jabareen, A reduced mixed finite-element formulation for modeling the viscoelastic response of electro-active polymers at finite deformation, Math. Mech. Solids 24 (5) (2018) 1578–1610.

[53] Z. Liao, M. Hossain, X. Yao, M. Mehnert, P. Steinmann, On thermo-viscoelastic experimental characterization and numerical modelling of VHB polymer, Int. J. Non-Linear Mech. 118 (2020) 103263.

[54] R. Bustamante, Transversely isotropic non-linear electro-active elastomers, Acta Mech. 206 (3–4) (2009) 237.

[55] R. Bustamante, J. Merodio, On simple constitutive restrictions for transversely isotropic nonlinearly elastic materials and isotropic magneto-sensitive elastomers, J. Eng. Math. 68 (1) (2010) 15–26.

[56] J.M. Ball, Convexity conditions and existence theorems in nonlinear elasticity, Arch. Ration. Mech. Anal. 63 (4) (1976) 337–403.

[57] A.J. Gil, R. Ortigosa, A new framework for large strain electromechanics based on convex multi-variable strain energies: Variational formulation and material characterisation, Comput. Methods Appl. Mech. Engrg. 302 (2016) 293–328.

[58] R. Ortigosa, A.J. Gil, A new framework for large strain electromechanics based on convex multi-variable strain energies: Conservation laws, hyperbolicity and extension to electro-magneto-mechanics, Comput. Methods Appl. Mech. Engrg. 309 (2016) 202–242.

[59] M.H. Siboni, R. Avazmohammadi, P.P. Castañeda, Electromechanical instabilities in fiber-constrained, dielectric-elastomer composites subjected to all-around dead-loading, Math. Mech. Solids 20 (6) (2015) 729–759.

[60] R. Ortigosa, A.J. Gil, C.H. Lee, A computational framework for large strain nearly and truly incompressible electromechanics based on convex multi-variable strain energies, Comput. Methods Appl. Mech. Engrg. 310 (2016) 297–334.

[61] R. Poya, A.J. Gil, R. Ortigosa, R. Sevilla, J. Bonet, W.A. Wall, A curvilinear high order finite element framework for electromechanics: From linearised electro-elasticity to massively deformable dielectric elastomers, Comput. Methods Appl. Mech. Engrg. 329 (2018) 75–117.

[62] M. Šilhavỳ, A variational approach to nonlinear electro-magneto-elasticity: convexity conditions and existence theorems, Math. Mech. Solids 23 (6) (2018) 907–928.

[63] J. Schröder, P. Neff, Invariant formulation of hyperelastic transverse isotropy based on polyconvex free energy functions, Int. J. Solids Struct. 40 (2) (2003) 401–445.

[64] M. Itskov, V.N. Khiêm, A polyconvex anisotropic free energy function for electro-and magneto-rheological elastomers, Math. Mech. Solids 21 (9) (2016) 1126–1137.

[65] S. Vetra-Carvalho, P.J. Van Leeuwen, L. Nerger, A. Barth, M.U. Altaf, P. Brasseur, P. Kirchgessner, J.-M. Beckers, State-of-the-art stochastic data assimilation methods for high-dimensional non-Gaussian problems, Tellus A 70 (1) (2018) 1–43.

[66] B. Benešová, M. Kružík, A. Schlömerkemper, A note on locking materials and gradient polyconvexity, Math. Models Methods Appl. Sci. 28 (12) (2018) 2367–2401.

[67] M. Horák, M. Kružík, Gradient polyconvex material models and their numerical treatment, Int. J. Solids Struct. (2020).

[68] J. Bonet, A.J. Gil, R. Ortigosa, A computational framework for polyconvex large strain elasticity, Comput. Methods Appl. Mech. Engrg. 283 (2015) 1061–1094.

[69] J. Bonet, A.J. Gil, R. Ortigosa, On a tensor cross product based formulation of large strain solid mechanics, Int. J. Solids Struct. 84 (2016) 49–63.

[70] J. Schröder, P. Neff, Poly-, Quasi- and Rank-One Convexity in Applied Mechanics, Vol. 1, Springer, 2010.

[71] I.-S. Liu, On representations of anisotropic invariants, Internat. J. Engrg. Sci. 20 (1982) 1099–1109.

[72] Q.-S. Zheng, Theory of representations for tensor functions—A unified invariant approach to constitutive equations, Appl. Mech. Rev. (ISSN: 0003-6900) 47 (11) (1994) 545–587.

[73] J. Schröder, D. Gross, Invariant formulation of the electromechanical enthalpy function of transversely isotropic piezoelectric materials, Arch. Appl. Mech. 73 (2004) 533–552.

[74] R. de Boer, Vektor-und Tensorrechnung für Ingenieure, Springer-Verlag, 1982.

[75] J. Bonet, A.J. Gil, R.D. Wood, Nonlinear Solid Mechanics for Finite Element Analysis: Statics, Cambridge University Press, ISBN: 1107115795, 2016.

[76] E.B. Tadmor, R.E. Miller, R.S. Elliott, Continuum Mechanics and Thermodynamics: From Fundamental Concepts to Governing Equations, Cambridge University Press, 2012.

[77] C. Miehe, D. Vallicotti, D. Zäh, Computational structural and material stability analysis in finite electro-elasto-statics of electro-active materials, Internat. J. Numer. Methods Engrg. 102 (10) (2015) 1605–1637.

[78] V. Ebbing, Design of Polyconvex Energy Functions for All Anisotropy Classes, Inst. für Mechanik, Abt. Bauwissenschaften, 2010.

[79] I. Fonseca, S. Müller, A-Quasiconvexity. lower semicontinuity, and young measures, SIAM J. Math. Anal. 30 (6) (1999) 1355–1390.

[80] M. Šilhavý, The Mechanics and Thermodynamics of Continuous Media, Springer, Berlin, 1997.

[81] R. Ortigosa, A.J. Gil, A new framework for large strain electromechanics based on convex multi-variable strain energies: Finite Element discretisation and computational implementation, Comput. Methods Appl. Mech. Engrg. 302 (2016) 329–360.

[82] J.M. Ball, Some open problems in elasticity, in: Geometry, Mechanics, and Dynamics, Springer-Verlag, 2002, pp. 3–59.

[83] J. Schröder, P. Neff, D. Balzani, A variational approach for materially stable anisotropic hyperelasticity, Int. J. Solids Struct. 42 (15) (2005) 4352–4371.

[84] N. Kambouchev, J. Fernandez, R. Radovitzky, A polyconvex model for materials with cubic symmetry, Modelling Simulation Mater. Sci. Eng. 15 (5) (2007) 451.

[85] P. Ciarlet, Mathematical Elasticity. Vol.I: Three-Dimensional Elasticity, North-Holland, Amsterdam, 1988.

[86] M. Gurtin, An Introduction to Continuum Mechanics, Acad. Press, New York, 1981.

[87] P.I. Galich, V. Slesarenko, S. Rudykh, Shear wave propagation in finitely deformed 3D fiber-reinforced composites, Int. J. Solids Struct. 110–111 (2017) 294–304.

[88] B. Wu, W. Zhou, R. Bao, W. Chen, Tuning elastic waves in soft phononic crystal cylinders via large deformation and electromechanical coupling, J. Appl. Mech. 85 (3) (2018).

[89] X. Zhao, Q. Wang, Harnessing large deformation and instabilities of soft dielectrics: Theory, experiment, and application, Appl. Phys. Rev. 1 (2) (2014) 021304.

[90] D.C. Stanier, J. Ciambella, S.S. Rahatekar, Fabrication and characterisation of short fibre reinforced elastomer composites for bending and twisting magnetic actuation, Composites A 91 (2016) 168–176.

[91] E. Allahyari, M. Asgari, Fiber reinforcement characteristics of anisotropic dielectric elastomers: A constitutive modeling development, Mech. Adv. Mater. Struct. (2021) 1–15.

[92] M. Al Kotob, C. Combescure, M. Mazière, T. Rose, S. Forest, A general and efficient multistart algorithm for the detection of loss of ellipticity in elastoplastic structures, Internat. J. Numer. Methods Engrg. 121 (5) (2020) 842–866.

[93] G. DeBotton, I. Hariton, E. Socolsky, Neo-Hookean fiber-reinforced composites in finite elasticity, J. Mech. Phys. Solids 54 (3) (2006) 533–559.

[94] M. Barchiesi, Loss of polyconvexity by homogenization: a new example, Calc. Var. Partial Differential Equations 30 (2) (2007) 215–230.

[95] V. Slesarenko, S. Rudykh, Microscopic and macroscopic instabilities in hyperelastic fiber composites, J. Mech. Phys. Solids 99 (2017) 471–482.

[96] F. Marín, J. Martínez-Frutos, R. Ortigosa, A. Gil, A convex multi-variable based computational framework for multilayered electro-active polymers, Comput. Methods Appl. Mech. Engrg. (ISSN: 0045-7825) 374 (2021) 113567.

[97] F. Marín, R. Ortigosa, J. Martínez-Frutos, A. Gil, Viscoelastic up-scaling rank-one effects in in-silico modelling of electro-active polymers, Comput. Methods Appl. Mech. Engrg. (ISSN: 0045-7825) 389 (2022) 114358.